THESIS FOR THE DEGREE OF LICENCIATE OF ENGINEERING

Incorporation and Characterization of Graphene Derivatives in Thermal Sprayed Coatings

PLINIO FERNANDES BORGES SILVA

Department of Industrial and Materials Science

CHALMERS UNIVERSITY OF TECHNOLOGY

Gothenburg, Sweden 2025

Incorporation and Characterization of Graphene Derivatives in Thermal Sprayed Coatings

PLINIO FERNANDES BORGES SILVA

Technical report no IMS-2025-3

Licentiate Thesis at Chalmers University of Technology

Department of Industrial and Materials Science

Chalmers University of Technology

SE-412 96 Gothenburg

Sweden

Tel: +46 (0)31 772 1000

Printed by Chalmers digitaltryck
Gothenburg, Sweden 2025

Incorporation and Characterization of Graphene Derivatives in Thermal Sprayed Coatings

PLINIO FERNANDES BORGES SILVA

Department of Industrial and Materials Science
Chalmers University of Technology

Abstract

This thesis explores the incorporation and characterization of graphene derivates in thermal spray coatings to enhance wear performance. Graphene nanoplatelets (GNP) and graphene oxide (GO) were integrated into alumina (Al_3O_2) and WC-Co-Cr matrices respectively, aiming to improve tribological performance and understand the mechanisms to their function as solid lubricants to improve the wear resistance. The study is based on three key scientific questions: the retention and functionality of GNP during wear testing, the effectiveness of molecular-level mixing in tailoring GO coatings on metal powders, and the viability of GO-coated powders made by molecular-level mixing in wear-resistant coatings produced by thermal spraying.

Synchrotron-based techniques, such as Scanning Transmission X-ray Microscopy (STXM) and X-ray Absorption Near Edge Structure (XANES) were employed and revealed that GNPs retained their structure after thermal spraying process. The experiment setup allowed the rotation of the sample relative to the X-ray beam, enabling the detection of GNPs aligned parallel to the sliding direction. After wear testing, amorphization of both the alumina matrix and GNPs was observed, indicated by an increased carbon content within the amorphized alumina regions.

A molecular-level mixing process was developed to coat GO onto metal powders, demonstrating the ability to control coating characteristics through variations in APTES and GO concentrations. This controllability was reflected in both the coverage and thickness of the GO coating on the metal powders, highlighting the process's capability to tailor the coating properties to meet specific application requirements.

The GO coating process was successfully applied to WC-Co-Cr porous powders, achieving GO deposition on both external surfaces and within the internal pores. These GO-coated WC-Co-Cr powders were then processed via thermal spraying, resulting in coatings with enhanced performance, including reduced porosity, lower coefficients of friction, and increased hardness. Raman spectroscopy and X-ray photoelectron spectroscopy (XPS) confirmed the retention of GO in both the sprayed coatings and wear tracks, even under different surface preparation conditions.

Key-words: Graphene-based materials incorporation, molecular-level mixing, metal powders, graphene distribution and interface, thermal spray coatings, wear resistance.

Preface

This licentiate thesis is based on the work performed in the Department of Industrial and Materials Science at Chalmers University of Technology from January 2022 to December 2024. The work was carried out under the supervision of Professor Uta Klement and Associate Professor Jinhua Sun. The examiner was Eduard Hryha. The work was funded by the Chalmers Foundation.

List of the appended papers:

PAPER A: Synchrotron X-ray Spectro microscopy analysis of wear tested graphene-containing alumina coatings

Antonio Mulone, Plinio Fernandes Borges Silva, Hui Yuan, Karina Thånell, Adam Hitchcock, Uta Klement

Carbon, Volume 227, Article 119245, 2024

https://doi.org/10.1016/j.carbon.2024.119245

PAPER B: Controllable Coating Graphene Oxide and Silanes on Cu Particles as Dual Protection for Anticorrosion

Jinhua Sun, Kristoffer H. Martinsen, Uta Klement, Alessandro Kovtun, Zhenyuan Xia, Plinio Fernandes Borges Silva, Eduard Hryha, Lars Nyborg, and Vincenzo Palermo

ACS Applied Materials & Interfaces, Volume 15, Issue 32

https://doi.org/10.1021/acsami.3c08042

PAPER C: Development of GO-Coated WC-Co-Cr Porous Powder for Improved Wear Resistance in HVAF Coatings

Plinio Fernandes, Jinhua Sun, Eric Tam, Stefan Björklund, Antonin Riche, Shrikant Joshi, Uta Klement

Submitted for publication

Contribution to the appended papers:

PAPER A: The author was part of the team that conducted the XANES synchrotron measurements at MAX IV. Following the measurements, the author performed the data analysis of both aluminum and carbon edges in collaboration with Antonio Mulone and Adam Hitchcock. The author wrote the paper in collaboration with the co-authors.

PAPER B: The author carried out the experimental work related to the Raman measurements and assisted in reviewing and revising the paper for publication.

PAPER C: The author performed the experimental work involving the GO coating process of the WC-Co-Cr powder. The HVAF spraying was carried out by Stefan Björklund, while the ball-on-disk tests were performed by Antonin Riche. The author did the characterizations and data analysis, and wrote the paper in collaboration with the co-authors.

Table of contents

Chapter I – Introduction

Motivation

Graphene, a single layer of carbon atoms arranged in a hexagonal lattice (chicken wire mesh), has attracted significant attention since its isolation from graphite in 2004 due to its exceptional properties, which include high tensile strength, Young's modulus, and electron mobility. These outstanding characteristics make it stronger than steel and an excellent conductor of both electricity and heat compared to conventional materials like copper [1,2]. Graphene's unique properties arise from its atomic structure, where each carbon atom forms covalent σ-bonds with three neighboring atoms, while a delocalized electron in the p_z orbital facilitates high electrical conductivity [3]. These features, along with a high surface area, corrosion resistance, and gas impermeability, make graphene an ideal material to reinforce ceramics, metals, and polymers-based composite in various fields [4–6]. Despite its potential, the full capabilities of graphene in composites are hindered by challenges such as the presence of defects, the difficulty of achieving high-quality graphene at large scale production, and issues with the dispersion and integration within the matrix material.

One promising area of research for graphene and its derivatives is their integration in metal matrix composites (MMCs), where they enhance properties such as thermal conductivity, wear resistance, and mechanical strength. Despite these advantages, challenges such as poor distribution and weak interfacial bonding between graphene derivatives and the metal matrix persist. In powder-based MMCs, various incorporation methods, such as in-situ growth [7] and ball milling [8], have been explored to prepare graphene reinforced composites. Furthermore, thermal spray technologies, particularly Atmospheric Plasma Spraying (APS) and High-Velocity Air Fuel (HVAF) spraying, have been identified as potential processes for creating graphene-reinforced coatings, offering enhanced performance in sectors such as aerospace, land base turbine blades, etc. [9,10]. However, the deposition process in thermal spraying must be carefully controlled to ensure the stability of the graphene and its integration into the final composite material.

Research objectives

The objective of this research builds upon the challenges of poor graphene distribution identified in Paper A, where limitations of the applied incorporation method through solution plasma spraying were shown insufficient to guarantee a well dispersed metal-graphene composite. In response, in Paper B, a GO-coating technique was developed to improve both distribution and interfacial bonding on metal powders, with the goal of enhancing the performance of the composite. Finally, in Paper C, the effectiveness of this GO-coating approach for wear-resistant applications is evaluated using HVAF spraying technology. This series of studies aims to find a more reliable route for graphene integration into wear-resistant coatings.

Research questions

The work of this thesis is based on the following research questions:

- Q1: To what extent can GNP maintain its structural and functional integrity after a wear testing to function as a solid lubricant in wear resistant thermal spray coatings?
- Q2: How effective is a molecular-level mixing process in achieving controllable graphene coatings on metal powders?
- Q3: Can the GO coated powder synthesized by the molecular-level mixing process be used to produce graphene containing wear resistance coatings via thermal spraying?

Chapter II – Background

Graphene and its properties

Graphene is a two-dimensional material consisting of a single layer of carbon atoms arranged in a hexagonal lattice, with a thickness equal to the size of a single carbon atom. The graphene's isolation in 2004 [11] was a benchmark for the research in carbon nanomaterials, establishing the research in 2D nanomaterials [12].

Graphene has a tensile strength of 130 GPa and a Young's modulus of 1 TPa, making it 200 times stronger than steel [2]. Graphene also has a 200 times higher electron mobility than silicon, being 200,000 $cm^2V^{-1}s^{-1}$ and 1000 $cm^2V^{-1}s^{-1}$. In comparison with Copper, Graphene has an electrical conductivity of 100 MS/m while Cu has 59 MS/m, and the difference in thermal conductivity is even greater, being 3,500 – 5,300 W/mK for graphene and 340 W/mK for Cu [13,14].

The exceptional properties of graphene are attributed to its atomic structure. The carbon atoms are arranged in a honeycomb lattice with a sp^2 hybridization. In the two-dimensional plane, each carbon atom forms covalent bonds, known as σ-bonds, with three neighboring carbon atoms. The fourth electron, however, remains in an unbonded, delocalized state in the p_z orbitals, which are oriented perpendicular to the plane of the carbon atoms. This delocalized electron is free to move through the p_z orbitals of adjacent carbon atoms forming π-bonds, a characteristic feature of aromatic compounds [15]. This atomic arrangement results in a highly stable in-plane structure, providing graphene with its exceptional mechanical properties. Simultaneously, the delocalized electrons are free to move throughout the entire graphene sheet, creating an efficient pathway for electrical and thermal conductivity. Other properties that have attracted significant research interest in graphene include its large surface area [16], anti-corrosion properties [17], and impermeability for most gases [18].

These remarkable properties are most effective at the nanoscale, making graphene a popular choice for reinforcing composites to enhance the properties of ceramic, metallic, and polymeric materials. Although the addition of graphene to composites has generally been successful in improving their performance, achieving the full potential of graphene-reinforced composites remains challenging.

One reason for this challenge is that the properties of graphene are highly sensitive to defects and functional groups or foreign atoms in its structure. The exceptional properties of graphene are obtained from single-layer, pristine graphene, without oxygen functional groups on its surface; however, producing such high-quality graphene on a large scale is difficult [19,20]. Additionally, the effectiveness of graphene in composites can be limited by its interaction with the matrix material and its distribution within the matrix. Even if the quality of the graphene is sufficient to ensure optimal properties, weak interface and poor distribution within the matrix can disrupt the synergy of properties, undermining the intended enhancements of the composite [21].

Synthesis of graphene and its derivatives

Since its isolation by Novoselov and Geim [11], graphene has gained significant attention, leading to extensive research interests on its production methods. For graphene-reinforced composites to be viable for real-world applications, it is essential that graphene can be produced on an industrial scale. Consequently, the development of cost-effective and efficient production processes capable of producing high-quality graphene has become a major focus for researchers and engineers.

Graphene manufacturing methods can be categorized into two different ways: top-down and bottom-up processes. Top-down methods involve exfoliating graphene layers from graphite through various methods and mechanisms. Mechanical exfoliation can be achieved by techniques such as micromechanical cleavage [11], liquid-phase exfoliation [22], ball milling [23], and fluid dynamics [24]. In addition to mechanical methods, chemical exfoliation, which involves the use of corrosive agents to delaminate graphite, has been developed as solution processing method for large-scale production. However, chemical exfoliation often results in oxidation of graphene with the presence of oxygen functional groups, either on the surface or at the edges of the graphene layers. The primary chemical exfoliation methods include electrochemical exfoliation [25] and the widely used Hummers' method [26], which has several modified versions. Figure 1 illustrates the structure of graphene with single-layer, and multi-layer structures and some derivatives produced by top-down

technologies such as graphene oxide, reduced graphene oxide and graphene nanoplatelets (GNPs) [27].

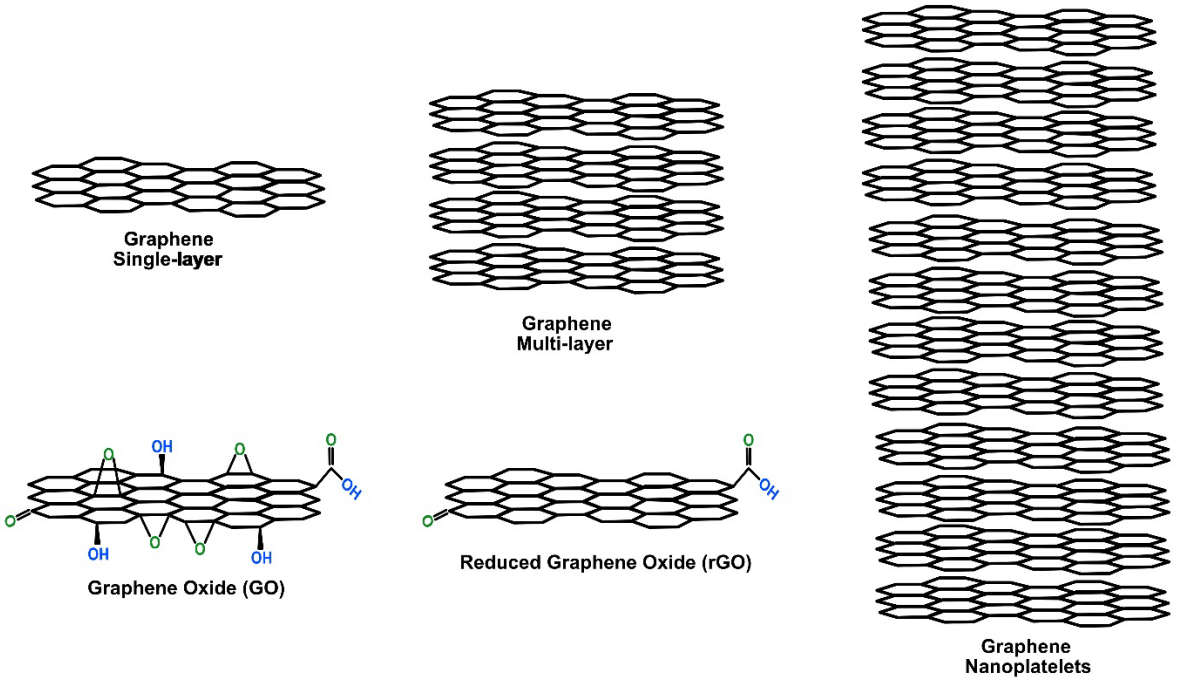

Figure 1: Graphene and its derivatives.

In contrast, bottom-up process involves synthesizing graphene from smaller molecules or carbon precursors. This is typically done by depositing carbon atoms from organic gases or substrate materials onto a surface to form graphene. The key variables in these processes include pressure, gas composition, substrate material, the use of catalysts, and temperature. Examples of bottom-up techniques include ultra-high vacuum (UHV) growth [28], molecular beam epitaxy (MBE) [29], and chemical vapor deposition (CVD) [30].

For large-scale industrial applications, top-down techniques present some advantages over bottom-up methods. The primary reason is the cost. Top-down methods typically utilize graphite as a precursor, along with standard chemicals or processes to exfoliate graphene. Although the cost of production remains higher than conventional materials, it is lower than bottom-up techniques, which often require special conditions such as vacuum or expensive substrates like copper. Another drawback of bottom-up techniques is the additional step required to transfer graphene from the growth substrate to the target material. While graphene produced through bottom-up methods

generally has fewer defects and minimal functional groups, the transfer process can alter or even damage the graphene.

Graphene oxide synthesis and properties

Graphene oxide, a widely studied derivative of graphene, is primarily produced through chemical exfoliation of graphite, with the most notable method being the Hummers' method, developed by William S. Hummers in 1958 [26]. This method involves exposing graphite to a highly acidic environment, followed by oxidation using strong oxidizing agents. Nowadays, the Hummers method is applied in the exfoliation of graphite into individual graphene oxide layers, functionalized with oxygen-containing groups. In the original Hummers' method, sulfuric acid (H_2SO_4) creates the acidic medium, while potassium permanganate ($KMnO_4$) and hydrogen peroxide (H_2O_2) act as oxidizing and neutralizing agents, respectively. Although the Hummers' method is widely used as the traditional route for producing GO, numerous modifications have been explored to improve efficiency, safety, and scalability [31–33].

In Hummers method, the exfoliation mechanism begins with H_2SO_4 intercalating into graphite, resulting in the increase of the distance between its layers, forming a graphite intercalation compound (GIC). This intermediate stage facilitates subsequent oxidation by $KMnO_4$, which penetrates the structure from the edges of GIC. Oxidation, progressing from the edges to the center, is diffusion-controlled, with evidence from Raman spectroscopy indicating higher oxidation at the edges compared to the core. Complete exfoliation into single-layer GO is achieved through sonication or vigorous stirring [34].

In addition to the edge-to-center oxidation mechanism, cross-plane oxidation can occur during chemical exfoliation. Pan and Aksay [35] explored this phenomenon by applying drops of oxidizing solutions onto highly ordered pyrolytic graphite (HOPG) to generate localized oxidation. This reaction led to the formation of epoxy groups, where oxygen atoms bonded with carbon atoms of the HOPG in a "triangular" configuration. The elastic strain energy generated by this bonding eventually surpasses the carbon interlayer interaction energy, causing cracking in the graphite structure. This cross-plane oxidation, combined with external mechanical input from sonication or stirring, significantly influences the lateral size of the GO produced.

GO is distinct from pristine graphene due to the presence of oxygen-containing functional groups on its surface. While graphene maintains a planar sp^2 hybridized structure, GO contains both sp^3 and sp^2 hybridization, resulting in a more tetrahedral configuration. The precise arrangement and distribution of these functional groups remains uncertain, largely because current analytical techniques struggle to provide localized measurements of the groups at high precision. Additionally, variations in production methods can introduce amorphous, nonstoichiometric features that further complicate the determination of GO's structure[36].

The modeling of GO's structure has a long history, beginning in 1939 when Hofmann and Rudolf [37] first suggested the presence of epoxy groups on the GO surface. In 1946, Ruess [38] built upon this model by incorporating hydroxyl groups. Further contributions were made by Scholz and Boehm [39], Nakajima and Matsuo [40], and He et al. [41], all of whom added information, including structures like C–O–C and C=C bonds. An schematic of these models are shown in figure 2.

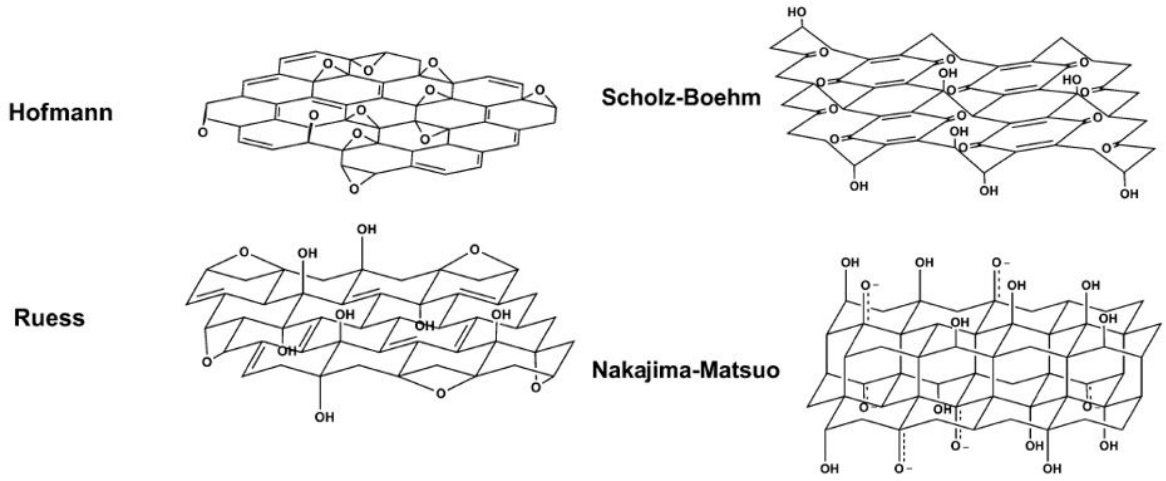

Figure 2: GO structure models. Adapted from Dreyer et al. 2010 with permission. [42]

The widely accepted model today was developed by Lerf and Klinowski [43] in 1998. Their model divides GO into two distinct regions: an aliphatic sp^3 region, where oxygen functional groups are concentrated, and an aromatic sp^2 region composed of intact graphene-like structures. The relative size and distribution of these regions depends on the degree of oxidation and, consequently, the synthesis method used. Although the exact positioning and distribution of functional groups are still debated, there is consensus on the types of functional groups present, which include hydroxyl (C–OH),

epoxy (C–O–C), carbonyl (C=O), carboxylic acid (O=C–OH), and conjugated double bonds (C=C). This combination of functional groups contributes to GO's unique properties and differentiates it significantly from pristine graphene [42]. Figure 3 presents the updated Lerf and Klinowski model with updated functional groups discovered afterwards.

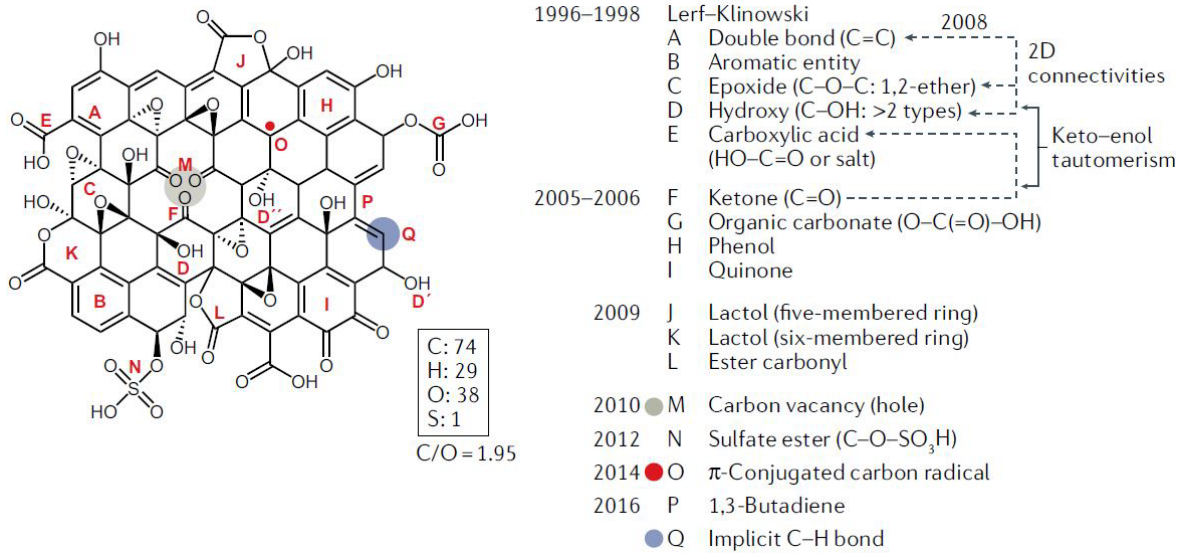

Figure 3: Current GO structure model with all possible functional groups. Adapted from Guo et al. 2022 with permission. [44]

These functional groups have significant impact on certain properties, such as electrical conductivity, but enhance GO's processability and compatibility with polymer, metal, and ceramic matrices [45,46]. Reduction of GO to produce reduced graphene oxide (rGO) improves its properties by partially removing the oxygen groups, yielding material characteristics that lie between GO and pristine graphene. Table 1 provides a comparison of key properties among pristine graphene, GO, and rGO:

Table 1: Comparison of the properties of graphene, graphene oxide and reduced graphene oxide

Property	Pristine Graphene [13]	GO [47]	rGO [48]
Electrical Conductivity	10^8 S/m	0.05 - 1 S/m	10^2 - 10^4 S/m
Mechanical Strength	130 GPa	40 - 70 GPa	100 - 150 GPa
Young's Modulus	1000 GPa	200 - 300 GPa	250 - 500 GPa
Optical Transparency	97.7%	70-90%	90-95%
Surface Area	2630 m²/g	700 - 1500 m²/g	1500 - 2500 m²/g
Hydrophilicity	Hydrophobic	Hydrophilic	Intermediate (depends on reduction level)

Graphene oxide reactivity and incorporation methods in composites

The primary advantage of incorporating graphene oxide (GO) into composites, compared to pristine graphene, lies in its increased chemical reactivity due to the presence of oxygen-containing functional groups. These groups, such as hydroxyl, carboxyl, and epoxide, provide multiple reactive sites that enable GO to chemically bond with a variety of composite matrices. This enhanced reactivity makes GO a versatile material in applications across different fields, allowing it to integrate with polymer, metal, and ceramic matrices more effectively than pristine graphene [42].

The chemical bonding between GO and matrix materials is typically governed by chemical reactions between the oxygen functional groups and the chemical groups on the surface of matrix. However, determining which specific functional groups are primarily responsible for bonding remains unclear. The selectivity of these groups in forming bonds with the matrix materials are not fully understood [44].

One prominent route for chemical bonding is through the epoxide group, which is one of the most abundant and reactive functional groups on GO. The epoxide ring structure is under elastic strain, making the carbon atoms in the basal plane more susceptible to nucleophilic attack (Fig. 4). When nucleophilic agents, such as amines (commonly used in epoxy polymer curing), react with the strained epoxide ring, a chemical bond forms between the nucleophile and the GO, while the oxygen in the epoxide is neutralized to form a hydroxyl group [49].

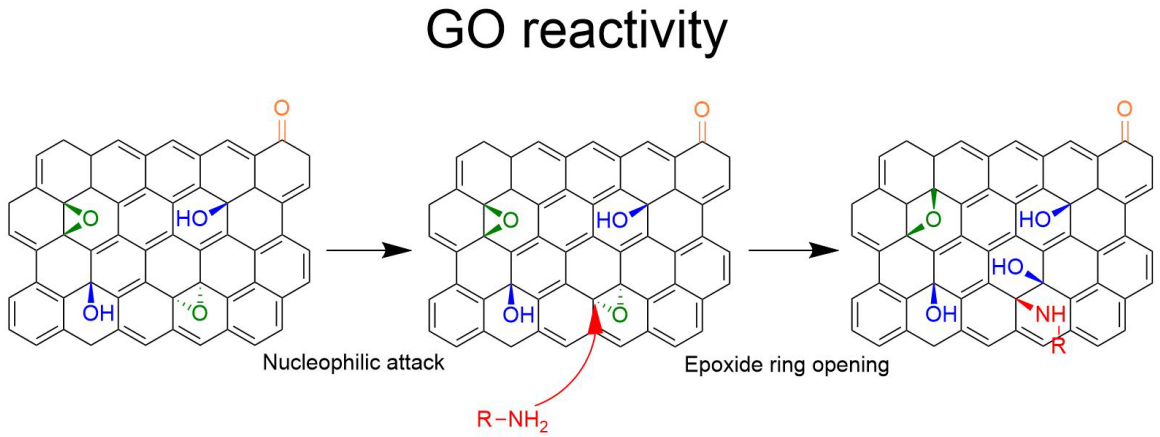

Figure 4: GO nucleophilic attack on epoxide functional group.

Hydroxyl groups on GO, while more stable than epoxides, also play a critical role in bonding, particularly in reactions involving organosilanes, which are used to form Si–

O bonds. This mechanism, illustrated in fig. 5, is common in the surface functionalization of materials like metal oxides, and similar reactions can occur in GO-based composites [50]. Interestingly, organosilanes containing amine groups can also react with epoxides, depending on the incorporation method, further expanding the possibilities for chemical bonding in GO composites [44].

Despite GO's high reactivity due to its oxygen-functional groups, the process of integrating GO into composite matrices remains complex. Issues such as poor distribution, common to many nanomaterial reinforcements, also arise in GO composites. Agglomeration of GO is mainly due to the strong interactions between its sheets, driven by van der Waals forces or π–π interaction, which are enhanced by the high surface energy of GO due to its large surface area [51]. These interactions cause the agglomeration of GO within the matrix.

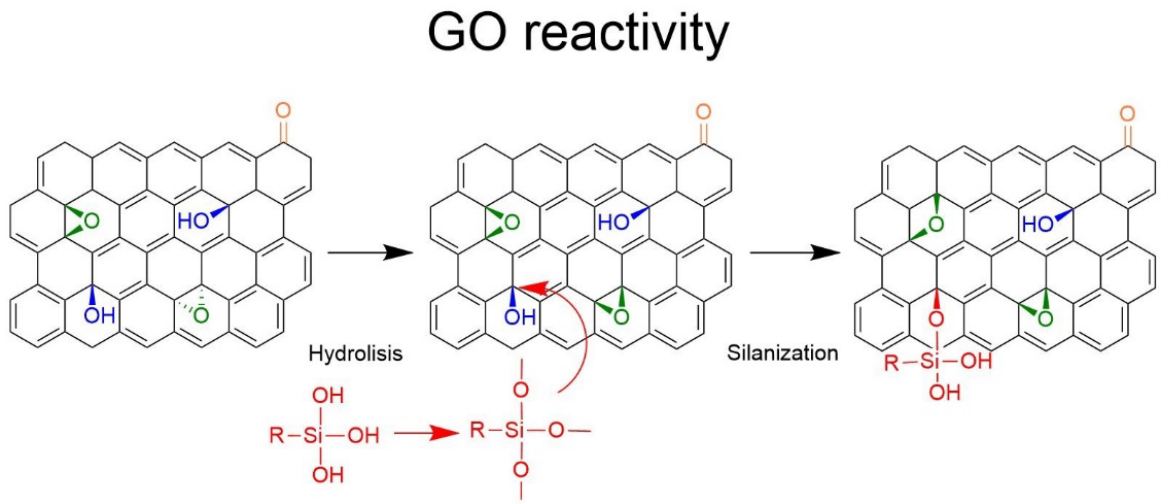

Figure 5: GO silanization on hydroxyl functional group.

Moreover, weak interfacial bonding can be attributed to the limited chemical compatibility between GO and certain matrices, especially hydrophobic ones. In such cases, there may be insufficient interactions between the GO's oxygen-functional groups and the matrix material. Poor wettability, particularly in high-viscosity matrices, can also contribute to inadequate adhesion between GO and the matrix [52]. Finally, GO's two-dimensional morphology introduces anisotropy, which can hinder the creation of effective mechanical interlocking sites, reducing the efficiency of stress transfer and thus limiting the mechanical reinforcement that GO can provide to the composite [53].

To address these challenges, the method of GO incorporation into composites is very important. Due to the wide range of available matrix materials, each composite presents unique challenges related to achieving optimal dispersion and interfacial bonding. Despite these variations, incorporation techniques can generally be classified into two categories: physical and chemical methods [53].

Physical methods rely on mechanical forces to achieve uniform dispersion of GO within the matrix. One widely used technique is ball milling, which is a straightforward, cost-effective, and scalable method. In ball milling, the matrix and graphene derivatives are placed in a sealed container along with milling balls. The process applies mechanical pressure, energy transfer, and increased temperature, resulting in a well-mixed composite powder. This method is well-established for the incorporation of graphene and its derivatives into various matrices. For instance, Guo et al. [54] utilized ball milling to integrate GNPs into an epoxy matrix, enhancing the composite's properties. Tan et al. [55] employed ball milling to create a ceramic composite cathode by mixing copper sulfide (CuS) with rGO for aqueous-hybrid-ion batteries, while Wang et al. [56] focused in using ball milling to incorporate graphene and multi-walled carbon nanotubes into Mg_2Ni alloy for hydrogen storage applications. However, ball milling has drawbacks, such as potential structural damage to GO sheets and partial reduction of oxygen-functional groups [57].

Mechanical stirring is another commonly used technique for incorporating graphene and its derivatives into composites. The stirring can be powered electrically or magnetically, and ultrasound waves can be applied in water baths to facilitate mixing. For example, Mahouri et al. [58] demonstrated how mechanical stirring, followed by sonication, was used to disperse GO and copper nanoparticles into an epoxy matrix. The mechanical stirrer was employed to achieve initial dispersion, while sonication helped break down any agglomerates formed during the process.

Chemical incorporation methods, such as solution mixing or the solvothermal method, represent another group of approaches. These methods involve the use of solvents, sometimes coupled with elevated temperatures, to dissolve both graphene oxide and the matrix material, promoting more homogeneous mixing. Additionally, chemicals can be added to enhance interactions between GO and the matrix. For instance, Kant and Sharma [59] synthesized α-Fe_2O_3/rGO nanohybrids using a simple solution mixing

method, without adding additional chemicals, by precipitating and drying α-Fe_2O_3 nanoparticles and then mixing them with an rGO suspension in water. In contrast, Guo and Bulin [60] fabricated a MgO/GO nanocomposite via the solvothermal method by adding magnesium acetate tetrahydrate (Mg precursor), polyvinylpyrrolidone (PVP), and GO in an aqueous solution, followed by heating the mixture in an autoclave at 180°C for 5 hours. The final composite was obtained by drying the precipitate at 300°C.

Self-assembly, also known as molecular-level mixing, represents another chemical approach for GO incorporation into composites. This method exploits the reactivity of GO's functional groups to form covalent bonds with the matrix through the use of small organic molecules, often referred to as coupling agents. These coupling agents play a crucial role in controlling the interface between GO and the matrix, making functionalization an important step in molecular-mixing methods. In this process, coupling agents are attached either to the matrix or GO to optimize compatibility [61]. For example, Sánchez-López et al. [62] utilized 3-aminopropyl-triethoxysilane (APTES) to functionalize the surface of biomedical-grade CoCr alloy, facilitating the adhesion of GO. In another study, Chen et al. [63] used a "bis-silane" solution containing dodecyltrimethoxysilane (DMTS) and tetraethyl orthosilicate (TEOS) to functionalize GO, also introducing benzotriazole (BTAH), a well-known anti-corrosive and hydrophobic agent. This approach was employed to create an anti-corrosion coating on pure copper by combining GO and BTAH.

Graphene reinforced metal matrix composites and applications

Metal matrix composites (MMCs) represent a well-established approach for enhancing the properties of metals by combining them with various reinforcing materials. This technique allows metals to benefit from the advantageous properties of other material classes, including ceramics, metal fibers, nanomaterials, and even natural residues [64]. Among the range of potential reinforcements, carbon-based materials, particularly graphene and its derivatives, offer significant advantages due to their high electrical and thermal conductivity, solid lubrication capabilities, and exceptional mechanical properties [65].

Graphene, due to its extraordinary properties, has gained significant attention as a reinforcement in metal matrix composites (GR-MMCs). The addition of small amounts

of graphene can significantly enhance the performance of these composites. However, achieving the full potential of graphene in MMCs remains a challenge due the problems already discussed before. Additionally, the manufacturing processes often involve high pressure and/or high temperature, which can damage the graphene flakes, further reducing the performance of the GR-MMCs [66].

A substantial part of the research in MMCs focuses on using metal powders or particles as the metallic matrix. This approach is beneficial due to the increased surface area of the powders, offering more sites for interaction with graphene compared to bulk metals [67]. Powder MMCs also create the possibility for additional graphene incorporation methods to be explored, including in-situ growth [68], and electrochemical deposition [12].

GR-MMCs powder can be used in different applications to enhance the properties of final components. The manufacturing processes typically involve a preliminary step of incorporating or admixing graphene with the metal matrix, followed by a process that consolidates the composite using the powder as feedstock. Some of the most common techniques that utilize metal powders include powder metallurgy, hot isostatic pressing, powder bed fusion (laser or electron beam), binder jetting, cold spray, and thermal spray. As mentioned before, these processes involve high temperature and substantial mechanical stresses (or kinetic energy), demanding a robust interface between graphene and metal powder to ensure graphene's stability and effectiveness in the final composite.

Thermal spraying of GR-MMCs

Thermal spray processing encompasses a range of technologies united by a common operating principle: they utilize electrical, chemical and/or kinetic energy to emit and attach a feedstock material onto a substrate, creating a coating. The feedstock supplied in powder, wire, or rod form is continuously fed during the process, which is heated and accelerated to form molten, semi-molten and solid particles. These particles are carried by a high-velocity gas flow toward the substrate, where they solidify rapidly upon impact forming splats. This rapid solidification allows each splat to act as a substrate for successive layers, gradually building the thickness of the coating [69].

The microstructure of thermally sprayed coatings is typically heterogeneous, influenced by both the feedstock properties and the process parameters. Variations in feedstock characteristics such as particle size distribution and morphology, rheological behavior, and surface oxidation are some characteristics of the feedstock that can vary during the thermal spray process and consequently introduce heterogeneity to the coating. On the other hand, process parameters such as carrier gas speed and purity, as well as nozzle size and shape, have a high influence in the splat formation. As a result, thermally sprayed coatings typically exhibit a lamellar structure characterized by anisotropy and defects such as porosity [70].

The primary markets for thermal-sprayed coatings are aerospace, industrial gas turbines, automotive, medical, and oil and gas extraction industries. These sectors employ thermal spray coatings for a range of purposes, including enhancing wear and corrosion resistance, providing anti-oxidation properties, acting as thermal barriers, increasing surface hardness, improving operational temperature thresholds, and, in medical applications, enhancing biocompatibility. In each of these applications, thermal spray coatings are applied to enhance and protect the surface of components, increasing their lifespan and durability without altering the mechanical performance of the bulk material [70,71].

The available thermal spray technologies differ significantly in parameters like feedstock delivery speed and gas temperature. These factors impact both the deposition rate of splats and the assurance of the splats to be adequately melted and adhered to the substrate. Broadly, thermal spray technologies are categorized based on the energy source used in the process—either electrical or chemical. Figure 6 illustrates a comparison of various thermal spray techniques, mapping them against process temperature and particle velocity to show the unique characteristics of each technology [72].

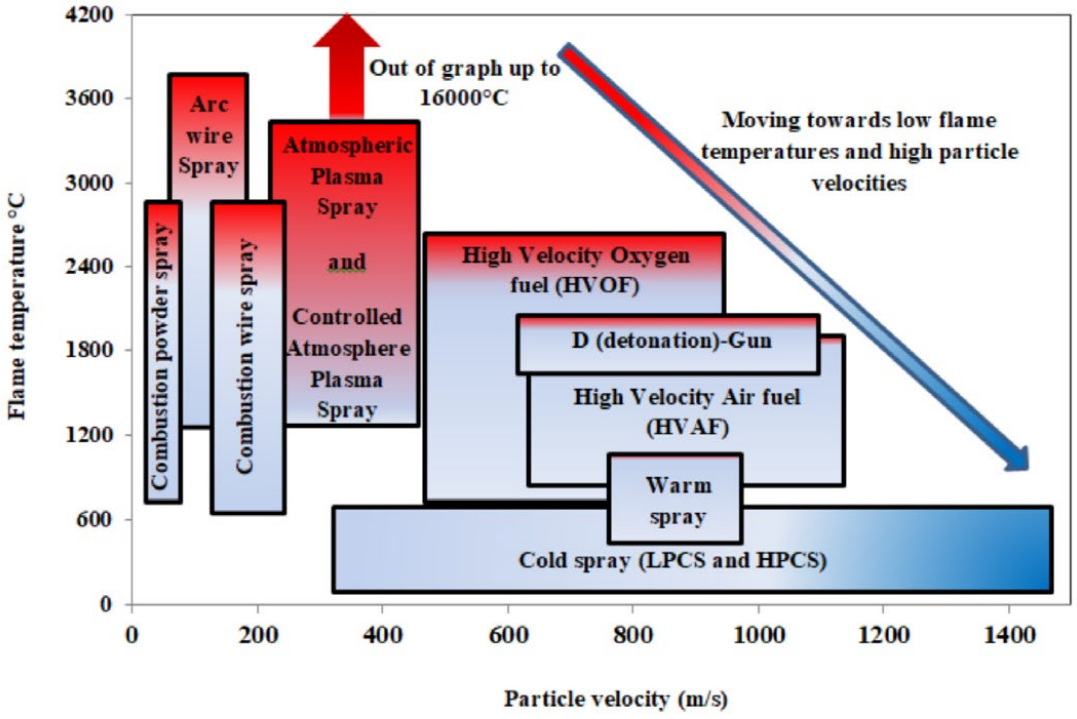

Figure 6: Summary of Thermal spray technologies regarding process temperature and particle velocity. Adapted with permission from [73]

One prominent example of high-temperature thermal spray technology is plasma spraying. This process utilizes ionized gas as both an energy source and a propellant to melt the feedstock and project it onto the substrate material. The gas is ionized in a plasma torch by an electric arc discharge, which elevates the internal pressure by expanding the gas, creating a jet of ionized gas that propels the molten material. Plasma spray systems can achieve temperatures ranging from 6,000 to 16,000 °C, making them suitable for melting various feedstock materials, typically powders or suspensions, a variant known as suspension plasma spray (SPS) [74].

For high-speed thermal spray techniques, High Velocity Oxygen Fuel (HVOF) is a widely recognized low-temperature method. In this process, fuel and oxygen gases are mixed in a combustion chamber, igniting and generating combustion. Powder feedstock is introduced to the combustion chamber via inert gas, where it expands with the combusted gases and builds pressure. As the gases exit through a nozzle, they accelerate, propelling the molten material toward the substrate at high velocities. HVOF is particularly well-suited for materials sensitive to elevated temperatures, such as carbides (e.g., WC-Co), which risk decarburization at temperatures above 3,000 °C. In some cases, to maintain a lower processing temperature and thus preserve the feedstock material, dry air is used instead of oxygen in a modified process known as

High Velocity Air Fuel (HVAF). This adjustment reduces the thermal energy applied to the material while still achieving high deposition speeds, making HVAF suitable for feedstock requiring extra thermal control [69,75].

Chapter III – Experimental work

Graphene oxide coating on powders

The graphene oxide (GO) coating process applied in this study is based on a developed molecular-level mixing approach. The procedure includes three steps: powder surface functionalization, GO incorporation, and drying. The initial surface functionalization involves applying a coupling agent (3-aminopropyl)triethoxysilane (APTES) onto the powder surface using toluene (Supelco, low water content) as a solvent. The concentration of APTES and the duration of mixing are key factors that determine the characteristics of the final coating. Following functionalization, the powder is washed with toluene to remove unreacted APTES, followed by water to eliminate residual toluene.

The GO incorporation step begins with dispersing GO paste in water to a concentration of 0.2 g/L. The GO, provided by LayerOne, was in an aqueous paste with a concentration of 10 wt%. The pH of the solution was adjusted to 7 by gradually adding ammonium hydroxide 1M solution (0.5–1 mL). The functionalized powder was vigorously stirred in water during the addition of the GO solution, and the mixture was left to stir for 5 minutes to ensure homogeneous coating. The powder was then rinsed with water and dried in a furnace at 40°C for 12 hours in air.

APTES was selected for this process due to its well-known role as a coupling agent between metal surfaces and GO. The structure of APTES includes a central silicon atom bonded to three ethoxy groups and one amine group, which facilitate chemical bonding with various species. Bond formation can occur through the amine group reacting with nucleophilic agents like hydroxyl or carboxyl groups, or through the hydrolysis of ethoxy groups to form silanol. Silanol groups can further bond through condensation with other nucleophilic agents [62]. While the precise mechanisms of bonding in the composite cannot be conclusively determined, it is known that metal oxide and hydroxide surfaces react with hydrolyzed silanol groups, and the amine group tends to react with the epoxy groups of GO [49,76]. Additionally, APTES can undergo self-condensation, forming Si-O-Si bonds either on the surface or in layers, potentially increasing the thickness of the APTES coating [77]. Figure 7 shows a

schematic of possible configurations of the APTES bonding between metal surface and GO.

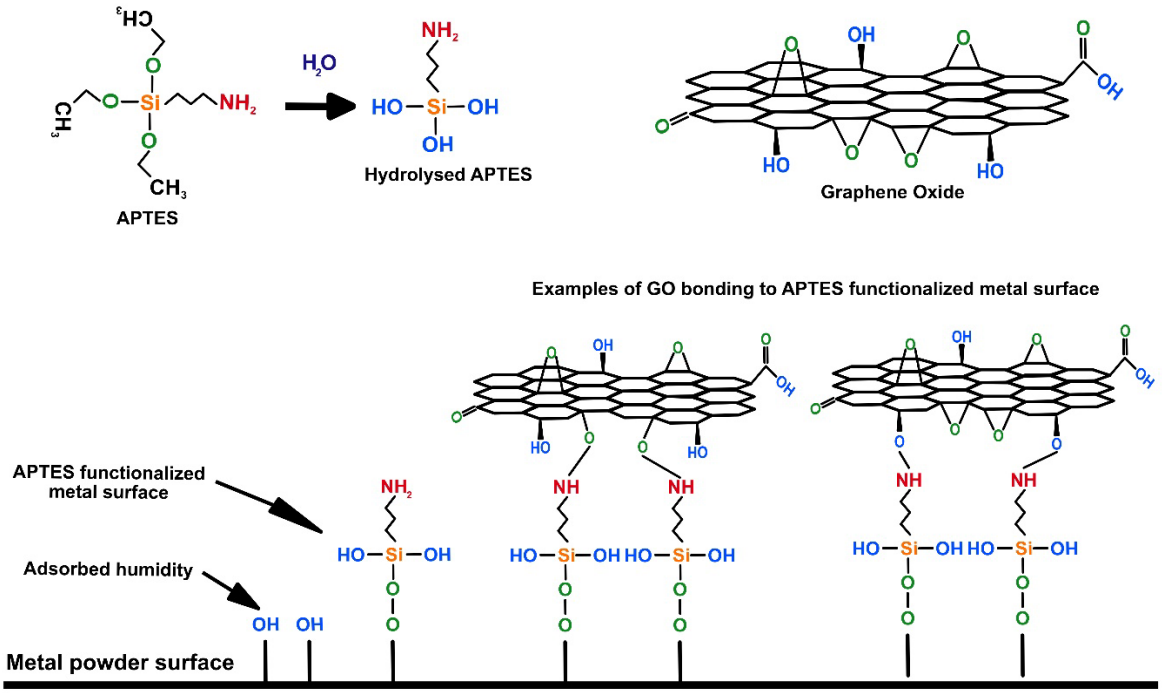

Figure 7: APTES mechanism of covalently binding metal surface to GO.

The solvent and water content are also critical factors in the reactivity of APTES. Water is required for the hydrolysis of ethoxy groups of APTES and for the formation of bonds with hydroxyl groups on the metal surface. However, an excess of water can lead to premature condensation of APTES, causing agglomeration. Toluene, with an ideal water content (around 0.15 mL per 100 mL), is an excellent solvent in this regard, as it maintains or extracts sufficient water on the substrate surface to facilitate the reaction [78,79]. In the case of metal powders, small quantities of water may already be present on the powder surface due to adsorption during handling or storage [80,81].

Thermal spray process

Two thermal spray technologies were used in this study, plasma spraying (Paper A) and high velocity air fuel HVAF (Paper C). Water-based alumina (Al_2O_3) suspension was obtained by Treibacher Industrie AG and water-based GNP suspension provided by 2D Fab AB were mixed in a proportion of 5 wt% of GNP over Alumina. Then, suspension plasma spraying was performed using an Axial III plasma torch and Nanofeed 350 suspension feeding system from Northwest Mettech Corporation (Mettech, Vancouver, Canada). Schematic is shown in fig. 8.

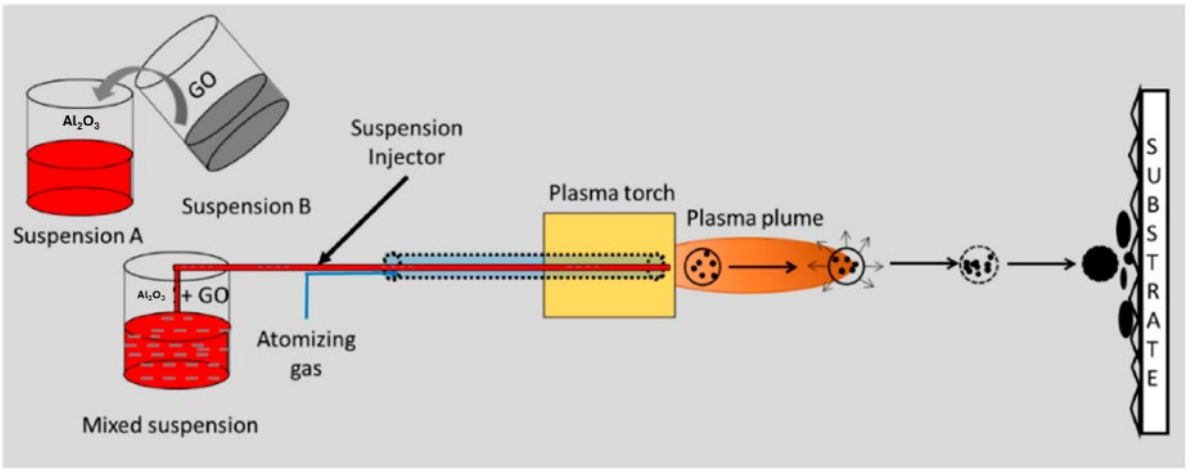

Figure 8: Schematic of the Suspension plasma spray used in this study. Adapted from [82]

For paper C, the spray gun used was M3, UniqueCoat Technologies LLC, Oilville, VA, USA. The parameters for the spraying experiment can be found in table 2:

Table 2: HVAF experiment parameters

Nozzle	5L4
Chamber	M3/3
Injector	#3
Air pressure PSI	113
Fuel 1 pressure PSI	105
Fuel 2 pressure PSI	115
Carrier gas l/min	60
Feeder (V1, V4, G4)	G4
Feed g/min	200
SoD standoff mm	300
Surface speed m/min	115
Step mm/rev	5

Materials characterization

Materials characterization techniques were employed to analyze both the GO-coated powders and the thermal-sprayed samples. Scanning Electron Microscopy (SEM) and Raman spectroscopy were the primary methods used to identify the presence of GO on the samples, as well as to qualitatively assess the coverage and thickness of the GO coating. To evaluate the stability of the GO coating at elevated temperatures, thermogravimetric analysis (TGA) was carried out. Experiments using various heating rates were also performed to simulate conditions relevant to manufacturing processes, such as thermal spraying. Additionally, X-ray Photoelectron Spectroscopy (XPS) was

used to assess the surface chemistry of the metal powder and to investigate the chemical bonding between the metal powder, APTES+GO.

For the GO-coated thermal sprayed samples, performance characterization was conducted to determine the effect of GO incorporation on the properties of the thermally sprayed coating. Dry-sliding wear tests were performed using a ball-on-disk tribometer to assess the tribological properties and the reduction in the coefficient of friction (CoF). The porosity of the thermal-sprayed coating was measured using optical microscopy, and relative density was determined through the contrast threshold method [61]. Vickers hardness testing was performed to evaluate the mechanical properties of the coating after the addition of graphene.

Finally, Scanning Transmission X-ray Microscopy (STXM) was applied to the thermally sprayed samples to analyze the microstructure and morphology of GNP within the coating, both before and after wear tests. This provided insights into the behavior of the GNP during the spraying process and their influence on the coating's performance.

Scanning Electron Microscopy

The scanning electron microscopy analysis was conducted using a Zeiss FEGSEM LEO-1550 instrument. SEM imaging played a key role in this study, both for characterizing the GO coating on powders and for verifying the presence of GO in the thermally sprayed samples. For both cases, an InLens detector was utilized, operating at a low acceleration voltage of 5 kV and a short working distance of less than 5 mm. These conditions were chosen to maximize the detection of the thin GO layer on the sample surface by enhancing contrast. The InLens detector, located along the electron beam path inside the chamber, is optimized to capture secondary electrons generated by the direct interaction between the primary electron beam and the sample. This setup enables high-resolution imaging of surface details, which is crucial for detecting the fine features of the GO coating. Figure 9 illustrates SEM images of the porous WC-Co-Cr particle virgin and with GO coating.

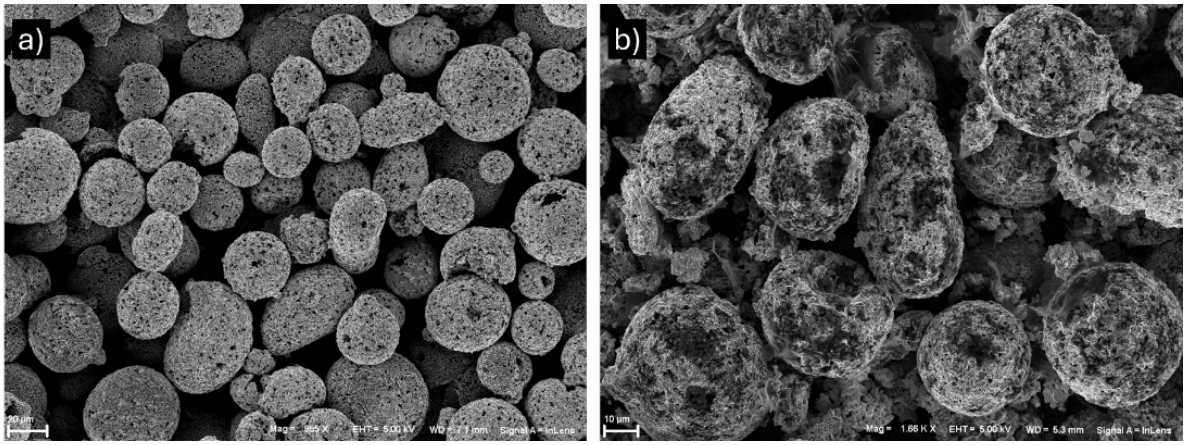

Figure 9: SEM of WC-Co-Cr, a) virgin, b) GO-coated

Raman spectroscopy

Raman spectroscopy is a widely used characterization technique for detecting carbon-based materials, including graphene oxide. Carbon materials exhibit strong sensitivity to visible light lasers, which excite molecules or phonons, leading to a shift in photon energy—either up or down—known as Raman scattering. This phenomenon provides insights into the vibrational modes of molecules within the sample. For carbon materials, two prominent peaks are consistently observed in Raman spectra: the D band at approximately 1350 cm^{-1} and the G band at around 1580 cm^{-1}. The G band originates from the stretching of C-C sp^2 bonds within the graphene plane, while the D band is associated with the vibration of sp^3 bonds in carbon, often indicating structural defects or, in the case of GO, the D peak can be attributed to the oxygen functional groups on the surface of the material.

In this study, Raman spectroscopy was extensively used to confirm the presence of GO and qualitatively assess the coverage of the GO coating on powder particles. Additionally, Raman analysis was performed on thermally sprayed samples to evaluate the integrity and survivability of the GO coating after the manufacturing process. Data collection was predominantly achieved through map scanning, where the laser scanned large sample areas, and filters were applied to generate contrast maps that indicated regions of higher graphene concentration. Figure 10 shows a raman map example along with the optical microscopy image of the respective region of analysis.

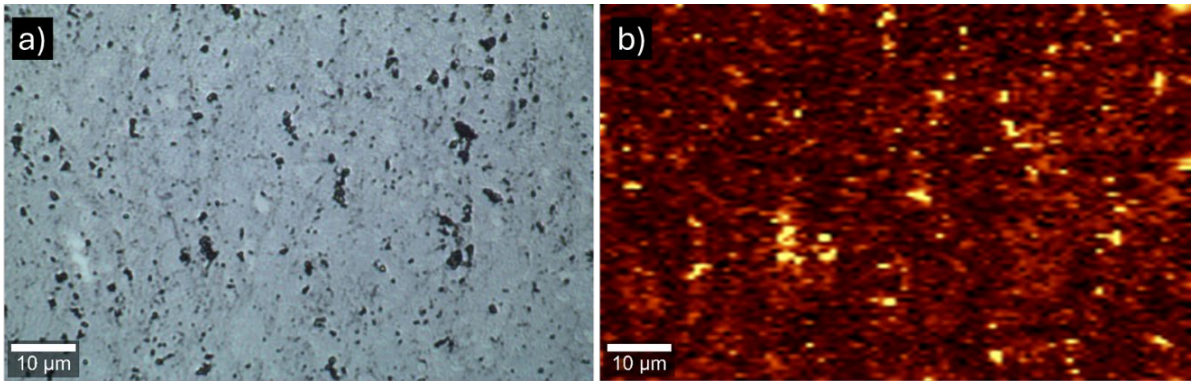

Figure 10: Raman mapping of the thermal sprayed GO-coated WC-Co-Cr cross-sectional polished sample. a) OM image b) Raman intensity map at 1580 cm^{-1} (G-band)

Thermogravimetry analysis

Thermogravimetric analysis was employed to investigate the thermal stability of GO coating at elevated temperatures. This analysis is particularly relevant because the manufacturing processes that utilize metal powders, such as thermal spraying, often involve high temperatures to consolidate the powders into final components. Given the importance of the GO coating's integrity during these processes, good thermal stability is a critical factor. Additionally, thermal spraying technologies are characterized by rapid heating rates, making it essential to evaluate how varying heating rates affect the stability of the GO coating.

To investigate these aspects, TGA experiments were conducted using a Mettler TGA/DSC 3+ instrument in an air atmosphere from room temperature to 900^{o} C, using different heating rates. This setup allowed for the measurement of the GO coating's thermal stability and its effect in the oxidation of the powder under conditions mimicking those experienced during high-temperature manufacturing processes.

X-ray Photoelectron Spectroscopy

The graphene oxide coating process developed in this study involves a surface chemistry reaction, and X-ray photoelectron spectroscopy was utilized to investigate the details of this method. XPS is a powerful technique that measures the energy of electrons emitted by the photoelectric effect when a focused X-ray beam strikes the sample surface. By analyzing the energy of these emitted electrons, which originate from a depth of no more than 10 nm, XPS provides detailed information about the elemental composition and chemical states of the surface compounds.

In this study, XPS was used first to elucidate the bonding interactions between copper powder, APTES, and GO in the coating process. The analysis allowed for the identification of the chemical bonds formed during the coating reaction, providing insight into the effectiveness of the APTES-GO coupling on the copper surface. Second, XPS was used to determine the chemical composition of the surface of virgin and GO-coated WC-Co-Cr thermal spraying coatings. In this case, XPS data helped to evaluate the stablity of the GO coating under drastic wear conditions and provided insights on the evolution of degradation and oxidation of the surface of the coatings. The PHI 5000 VersaProbe III Scanning XPS Microprobe was employed for both analysis, using a monochromatic Al Kα X-ray beam with an emission energy of 1486.6 eV and a focused beam diameter of 0.1 mm to perform high-resolution surface characterization.

Thermal sprayed coating characterization

To evaluate the impact of graphene oxide on thermal spray coatings, optical microscopy (OM) imaging and microhardness testing were employed. Both methods were conducted on as-spayed cross-sectioned, polished samples prepared from GO-coated and uncoated (virgin) powders processed via thermal spraying. Optical microscopy provided data on the relative density of the coatings through image analysis, which enabled the identification and quantification of pore areas based on contrast differences. The images were captured using a Zeiss AxioVision 7 microscope, equipped with a Zeiss digital camera 35 and AxioVision software.

Microhardness testing was performed to assess the mechanical properties of the coatings, particularly with regard to the influence of GO addition. Hardness is a critical factor for wear-resistant applications, and the aim of adding GO, functioning as a solid lubricant, was to maintain the high hardness of the WC-Co-Cr sprayed coating without compromising its mechanical integrity. Hardness measurements were carried out using a Struers Durascan 70G5 (Ballerup, Denmark) under a 500 g load. For each sample, ten indentations were made, and the average hardness values were reported to ensure reliable results.

Dry sliding wear testing

Wear refers to the progressive degradation of material surfaces due to mechanical or chemical interactions with other materials or surfaces. This degradation leads to the detachment of material from the surface in the form of particles, known as wear debris. As wear debris accumulates, it can further contribute to surface erosion, accelerating the wear process and potentially leading to system failure. The wear rate is influenced by several factors, including material properties (such as hardness and roughness), the nature of contact (e.g., stationery or moving), movement type (e.g., sliding or rotating), and the presence or absence of lubricants. These variables determine the wear mechanism and ultimately the lifespan of the component. [83].

The ball-on-disk test (BoD) is a standard tribological method for assessing material wear resistance. In this test, a pin typically with an interchangeable sphere that can be replaced with different materials to suit the hardness of the sample under analysis, is pressed against a disk-shaped sample at a controlled compressive force, either constant or variable. This arrangement allows for consistent contact between the pin's surface and the sample. The pin and disk pair are then subjected to relative motion, either as linear back-and-forth movement or as rotation within a set diameter. Both the compressive force applied to the pin and the resistive force generated by the sample's friction are recorded throughout the test, enabling the calculation of the coefficient of friction for the material in analysis [84]. A schematic of a ball-on-disc wear test is depicted in fig. 11:

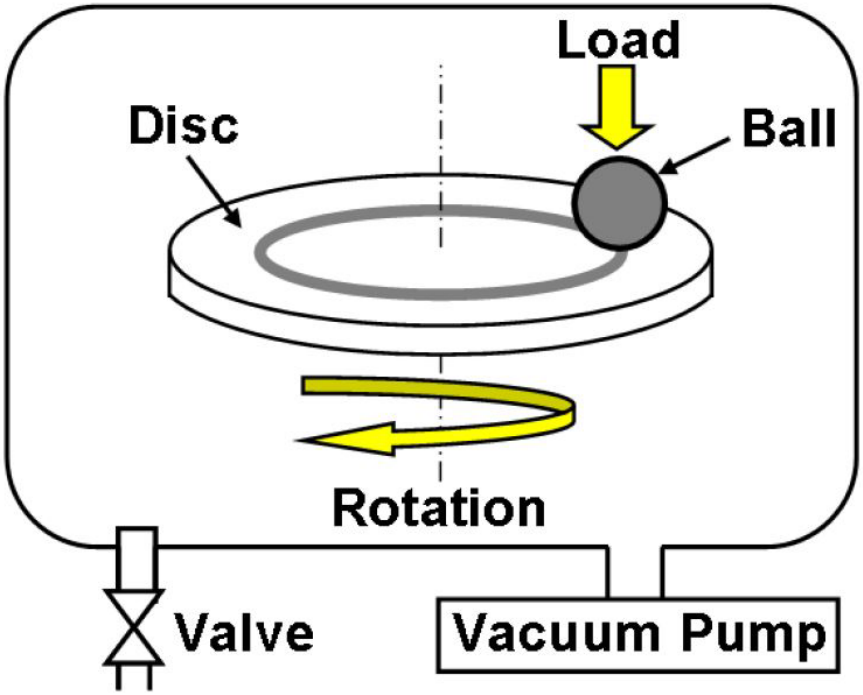

Figure 11: Ball-on-disk wear test schematic. Adapted with permission from [85]

The evaluation of the impact of GO coatings on wear resistance and the CoF of thermal-sprayed samples was performed using a ball-on-disk test and specific wear rate (SWR) measurements. Testing was carried out on a TRB3 ball-on-disk tribometer from Anton Paar. Both virgin WC-Co-Cr and GO-coated samples were tested in as-sprayed, ground, and polished conditions, resulting in a total of four sample variations. Testing parameters for all samples are summarized in table 3.

Table 3: Parameters used for BOD tests.

Normal Load (N)	Sliding Distance (m)	Linear speed (m/s)	Radius (mm)	Ball
20	5000	0,2	9	Alumina

Scanning Transmission X-ray Microscopy

Scanning Transmission X-ray Microscopy (STXM) is a sophisticated technique that integrates both microscopy and spectroscopy, typically conducted at synchrotron beamlines. It allows for imaging of very thin samples by scanning them with a focused X-ray beam. The beam's energy is adjusted within a specific range, where the sample selectively absorbs X-rays according to the chemical state or crystalline structure of its components. These specific energy ranges, known as "edges," correspond to the

absorption characteristics of certain chemical elements. Different chemical states or structural organizations of an element absorb X-rays at slightly different energy levels, allowing the technique to differentiate between them. This process is known as X-ray Absorption Near Edge Structure (XANES), or Near Edge X-ray Absorption Fine Structure (NEXAFS). These techniques produces a series of images, called "stacks," which enable the identification of different chemical phases or states in distinct regions of the sample.

In this study, both STXM and XANES experiments were carried out at the SoftiMAX beamline at MAX IV and at the SpectroMicroscopy beamline (10ID1) at the Canadian Light Source (CLS). Sample preparation involved creating electron-transparent lamellae using Focused Ion Beam (FIB) milling. For the Al Kα edge, a FEI Versa 3D with a Ga+ ion source was used, while for the C Kα edge, a Thermo Scientific Helios 5 PFIB UXe DualBeam Plasma FIB equipped with a Xe+ ion source was employed.

Chapter IV – Results and summary of appended papers

In this chapter, the research questions proposed in chapter I are addressed by a summary of results from the appended papers. Research question Q1 was explored in paper A, Q2 was examined in detail in paper B, and research question Q3 was addressed in paper C.

Paper A: Synchrotron X-ray Spectro microscopy analysis of wear tested graphene-containing alumina coatings

The addition of GNP into alumina coatings during thermal spraying was already investigated in a previous study [86], demonstrating improvements in the coefficient of friction. However, GNPs were not detected in the wear track after the dry sliding test. Hence, to address the condition of the GNPs before and after wear tests, scanning transmission X-ray microscopy and X-ray Absorption Near Edge Structure were used to analyze the structural configuration and perform chemical analysis of the GNPs within the as-sprayed matrix and the wear track.

The as-sprayed sample was examined to establish a reference for the structural displacement and chemical composition for both alumina matrix and GNP particles. The Al K-edge analysis revealed 3 different alumina structures phases: α-alumina, γ-alumina, and amorphous alumina (Fig. 12 a). Alpha-alumina appeared as round grains, well distributed throughout the sample (highlighted in red). Gamma and amorphous alumina phase (green and blue, respectively) were irregularly shaped, acting as a filling structure between the alpha-alumina grains.

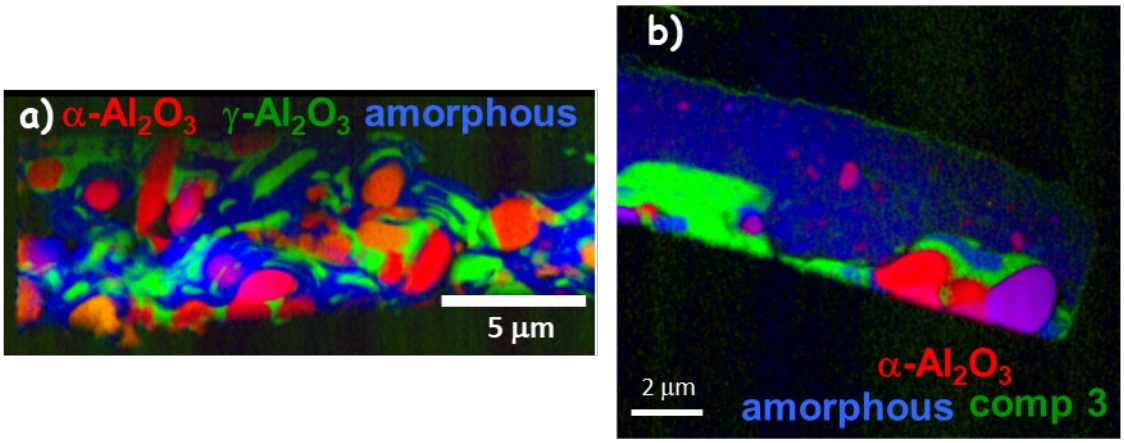

Figure 12: STXM of Al K-edge. a) Phase composition map of the as-sprayed sample. b) Phase composition map of the wear track sample

After the wear test, the structure of the alumina matrix was modified, and mostly amorphous alumina was present (Fig. 12 b). This indicated that the ball-on-disk test was rather harsh and that the applied pressure caused the amorphization of part of the alumina structures below the wear track.

Figure 13 shows the configuration of GNP in the alumina matrix in the as-sprayed sample. After the thermal spray process, the GNP preserved as clusters in between the alumina matrix. By a rotation of the sample inside the STXM chamber, the orientation of the GNPs were detected to be mostly parallel to the sample's surface.

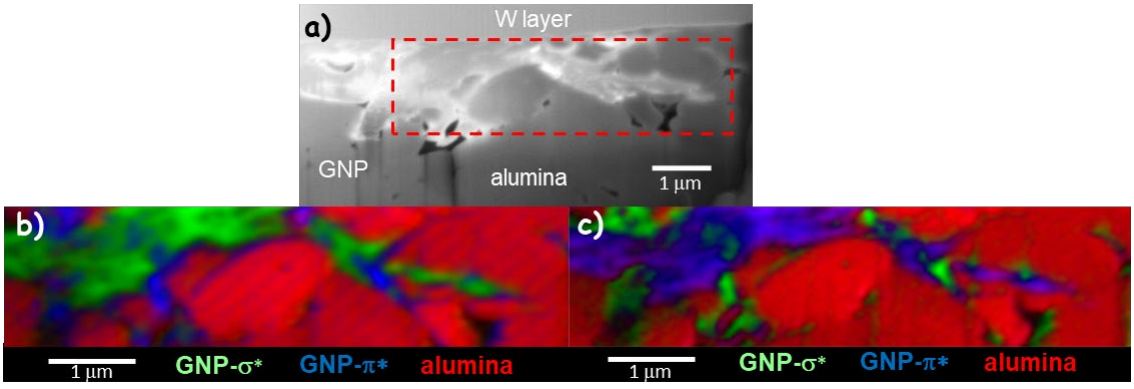

Figure 13: STXM of C K-edge of the as-sprayed sample. a) STXM image of the region of interest, GNP has a bright contrast. b) Phase composition map at horizontal position. c) Phase composition map at vertical position.

In the wear track sample, the GNP signal was detected in concentrated areas near the surface, adjacent to the tungsten protective layer (Fig. 14 b). This result confirms the hypothesis of GNPs acting as a solid lubricant in wear resistant applications, However, a sharp and intense peak at the carbon absorption range was also identified in the alumina matrix (Fig. 14 c). This peak can be related to amorphous configurations of

carbon, such as amorphous carbonate. Therefore, this phenomenon indicates that along with the alumina matrix, part of the GNP went through amorphization, and it was dissolved in the amorphous alumina phase.

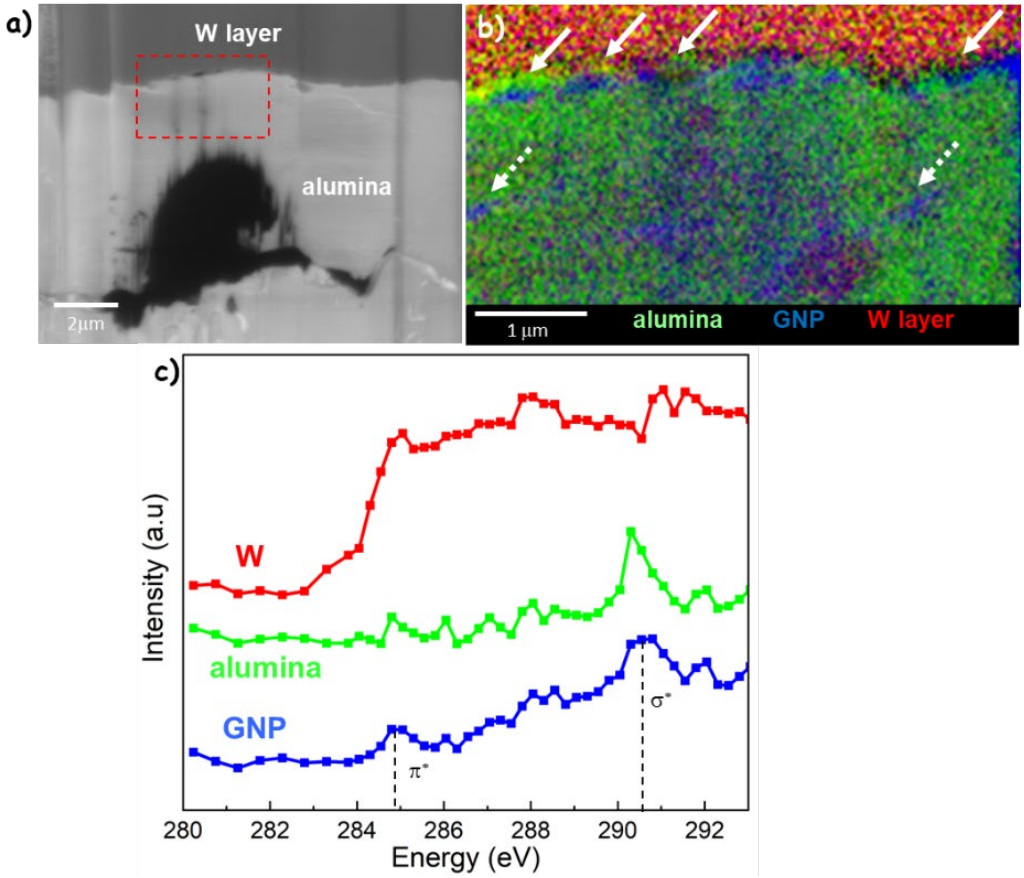

Figure 14: STXM at C K-edge of the wear track sample. a) SEM image of the area of interest. b) Phase composition map. c) XANES data from the area of interest.

STEM-EDS analysis was performed on the wear track sample, targeting amorphous alumina regions and α-alumina grains, as shown in Fig. 15. It could be shown that the amorphous alumina regions had a 4 times higher carbon concentration compared to the α-alumina grains. These findings validate the structural and functionality retention of GNP after both thermal spray and wear testing. However, the ball-on-disk test may imposed significant mechanical stresses on the sample, causing amorphization on both alumina matrix and GNPs.

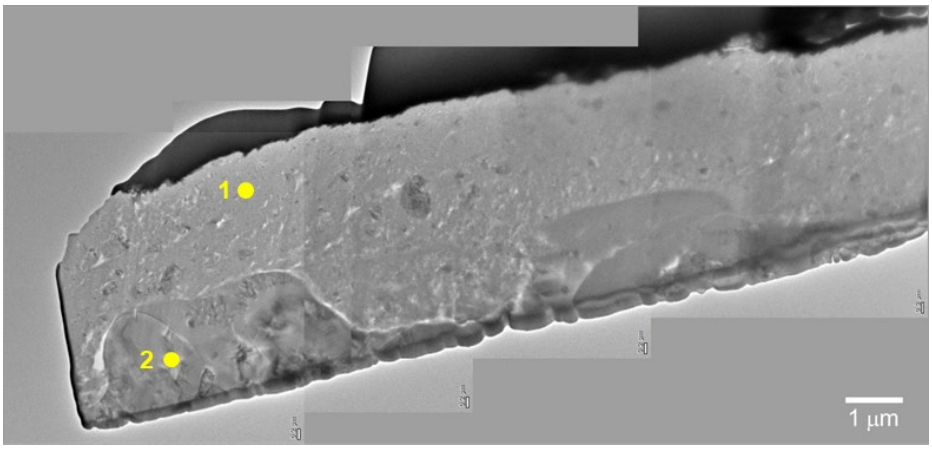

Figure 15: STEM-EDS image with points of analysis. 1) Amorphous region. 2) α-alumina grains.

Paper B: Controllable Coating Graphene Oxide and Silanes on Cu Particles as Dual Protection for Anticorrosion

The incorporation of graphene and its derivatives into thermal spray coatings showed a promising strategy for improving the wear resistance of coatings. However, the mixing of GNPs and alumina powder did not provide a uniform distribution. Therefore, molecular-level mixing was used to chemically bond graphene oxide to metal powder surfaces using a coupling agent, APTES. This approach aimed to improve GO distribution, strengthen the interface of the GO with the matrix, and enable precise control of the GO coating characteristics. In this study, spherical pure copper was selected as the base metal powder.

To evaluate the efficiency of the developed process, two experimental parameters were investigated: the concentration of APTES during the surface functionalization step and the GO solution concentration during the incorporation phase. The results demonstrated that APTES concentration played a critical role in determining the extent of GO coverage on the metal powder surface. At low APTES concentrations (e.g., 0.05 vol%), the functionalization layer was incomplete leading to partial GO coverage during the incorporation step. On the other extreme, high APTES concentrations produced a thick functionalization layer, resulting in full coverage and thick coating GO on the powder surface. SEM analysis on the different samples (Fig. 16) revealed this progression, with white wrinkles indicating GO presence.

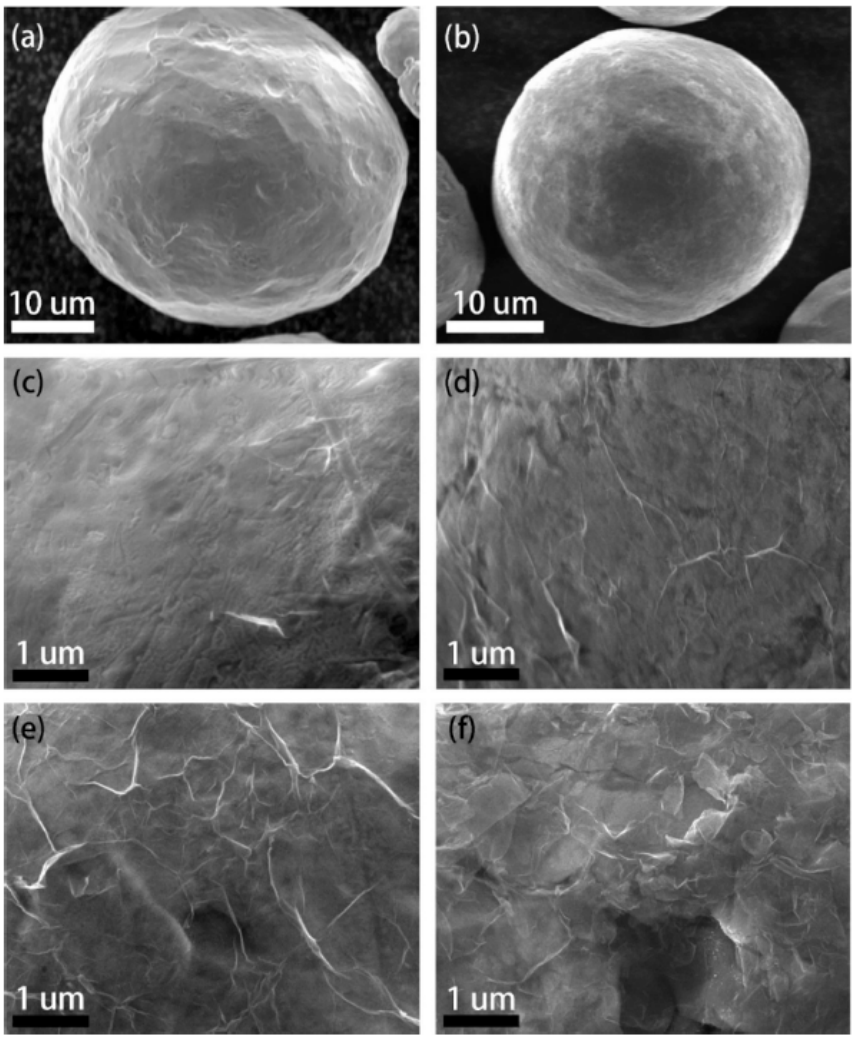

Figure 16: Molecular-level mixing coating process evolution. a) Pure Cu as received. b) APTES surface functionalized Cu. GO-coated Cu with APTES concentration of c) 0.05% d) 0.2% e) 0.8% and f) 1.5%

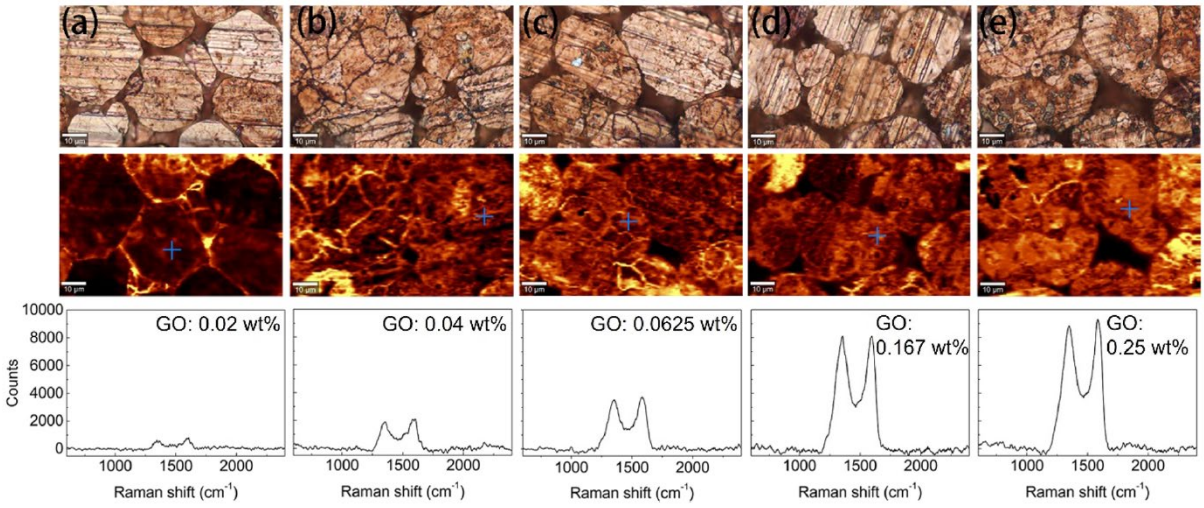

Figure 17: OM images (first row), Raman maps (second row), Raman spectra (third row) of compressed GO-coated Cu powders applying different GO solution concentrations. a) 0.02 wt% b) 0.04 wt% c) 0.0625 wt% d) 0.167 wt% e) 0.25 wt%

Similarly, the GO concentration during the incorporation phase significantly influenced the coating thickness and uniformity. At low concentrations, all the water dispersed GO particles were absorbed by the functionalized surface of the powder. However, they were not enough to cover all the available reaction sites, leaving part of the surface only coated with APTES. Increasing GO concentration, full coverage is achieved resulting in the formation of wrinkles across the entire surface. At even higher GO concentrations, the presence of more wrinkles indicates the formation of stacked multilayer GO. A saturation point was observed at 0.25 wt%, as unabsorbed GO was observed in the water solution after the incorporation step. Raman spectroscopy (Fig. 17) confirmed the increased GO thickness, evidenced by higher D and G band intensities at elevated concentrations. Raman mapping further verified the uniformity and extent of GO coverage. Hence, the molecular-level mixing proved to be able to produce GO coated powders with controllable characteristics such as full or partial coverage, thick or thin coating.

Paper C: Development of GO-Coated WC-Co-Cr Porous Powder for Improved Wear Resistance HVAF Coatings

The developed GO coating process was successfully applied to WC-Co-Cr porous powder, demonstrating the versatility of the method. The porous nature of the powder imposed an additional challenge, as the process had to apply the GO coating not only on the external surface but also the internal surfaces of open pores. This coated powder was afterwards used in a thermal spray process to create wear-resistant coatings. Ball-on-disc testing was performed to evaluate the performance of the graphene-containing coating compared to the initial WC-Co-Cr coating. X-ray photoelectron spectroscopy (XPS) was employed after the wear tests to confirm the presence and the state of GO.

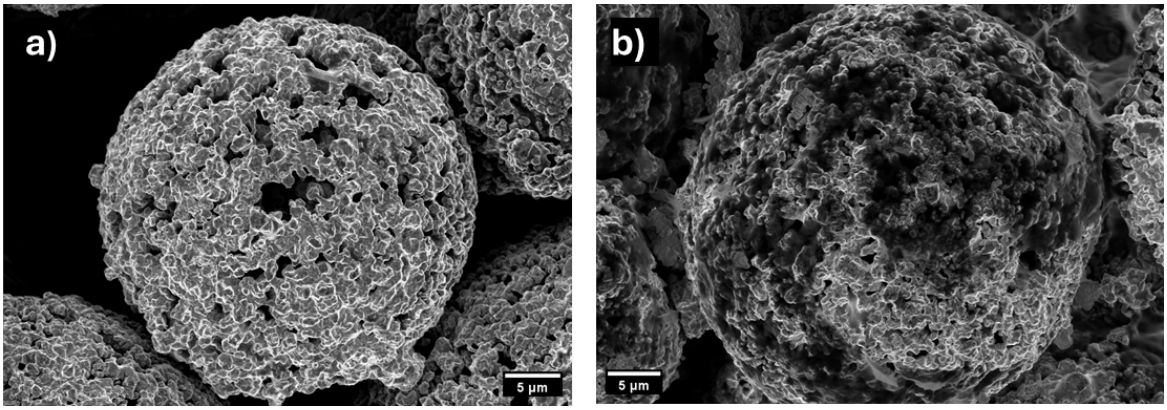

Figure 18: WC-Co-Cr porous powder. a) Virgin powder. b) GO coated powder.

Using the molecular-level mixing process, a partial GO coating was applied on both external and internal surfaces of the WC-Co-Cr powder. The partial coating was of interest in this experiment, since fully covered particles could hinder the densification of the sprayed coating by reducing direct contact between WC-Co-Cr particles. Figure 18 shows SEM images of the virgin WC-Co-Cr powder, and the GO coated WC-Co-Cr powder. Raman spectroscopy mapping on cross-sectioned powder particles (Fig. 19) confirmed the presence of GO within the internal pores, identifying the presence of intense peaks (bright regions highlighted in Fig. 19 b) in these regions.

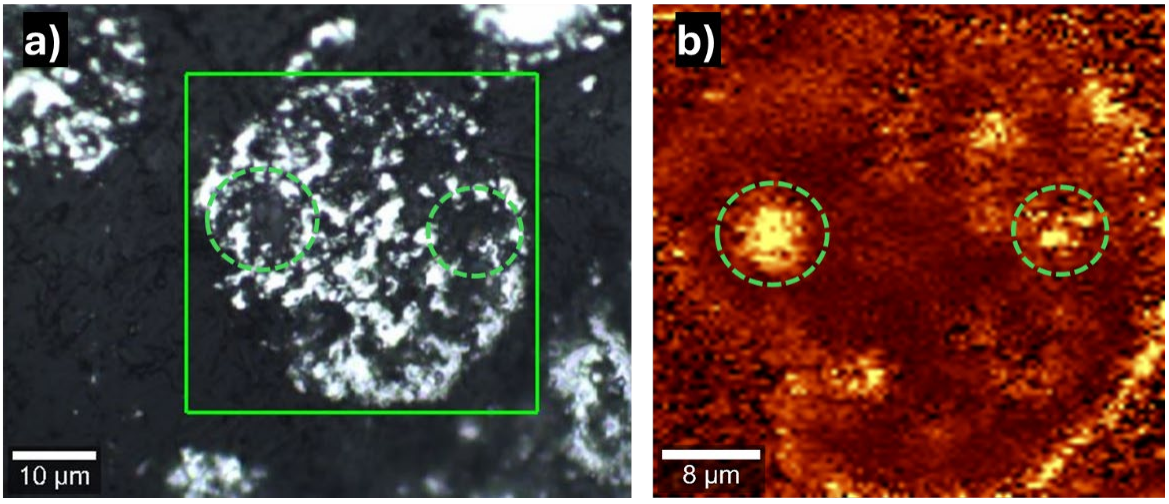

Figure 19: Cross-sectioned powder particle of GO-WC-Co-Cr powder. a) OM image, area of analysis and pores highlighted in green. b) Raman mapping with pores highlighted in green.

Both WC-Co-Cr and GO-WC-Co-Cr powders were submitted to a thermal spraying process to fabricate wear resistant coatings, which were tested under ball-on-disc tribometer conditions. The test was first conducted on the as-sprayed coatings to evaluate and compare the performance of the coatings. The GO-WC-Co-Cr coating exhibited superior performance, reducing the CoF of the sample throughout the test,

as shown in Fig. 20. This result validates the effectiveness of the developed process in producing powder feedstock for thermal sprayed wear resistant coatings.

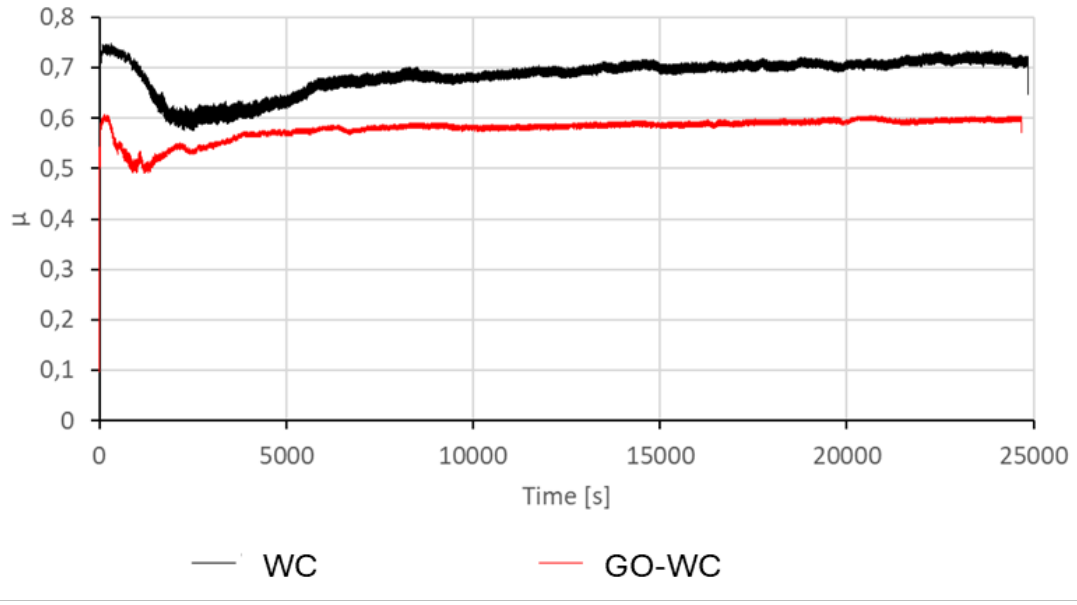

Figure 20: Dry sliding wear testing of the samples.

To further investigate the retention of GO in the thermal sprayed coatings after wear testing, XPS was used to study the surface chemical composition within the wear track. Samples with different surface conditions were analyzed to determine the evolution of the degradation of the surface. Different surface conditions were looked upon and table 4 presents the chemical compositions, which consistently identified the π-π bond peak, characteristic of carbon nanomaterials, across all samples [87]. In addition, the chemical composition of the GO coating changed, showing a progressive increase in oxidized chemical states (Table. 4.b) as surface degradation applied to the samples intensifies. These findings confirm the presence of GO in the thermal sprayed coatings after different wear conditions and surface treatments. Table 4.c summarizes the chemical compositions of the reduced and oxidized states analyzed in the samples.

Table 4: XPS overall carbon chemical composition on the surface of the GO coated samples.

A	**Reduced states**				
Chemical states	WC	M-C	sp2-C	sp3-C	π-π*
Binding energy (eV)	282.7	283.6	284.5	285.2	*>291.0*
GO-WC (Powder)	4.25%		21.00%	12.00%	<0.5%
GO-WC (As-sprayed)	3.50%	5.00%	21.50%	2.00%	<0.1%
GO-WC (Polished)	9.00%	3.50%	19.50%	8.00%	0.50%
GO-WC (50 µm grounded)	2.00%		2.00%	14.50%	<1.0%
B	**Oxidized states**				
Chemical states	sp2-C-O	sp3-C-O	C=O	COO-	CO32-
Binding energy (eV)	*285.5 – 286.5*	286.5 – 287.	287.5 – 288.5	289.0 – 290.	290.5
GO-WC (Powder)	8.50%	4.25%	2.00%		
GO-WC (As-sprayed)	1.00%	1.50%	1.00%		
GO-WC (Polished)	5.00%	3.00%	2.50%	1.00%	<0.5%
GO-WC (50 µm grounded)	7.50%	11.50%	8.50%	5.00%	2.00%

C	**Summary of chemical states**	
Samples	**Reduced states**	**Oxidized states**
GO-WC (Powder)	37.25%	14.75%
GO-WC (As-sprayed)	32.00%	3.50%
GO-WC (Polished)	40.50%	11.50%
GO-WC (50 µm grounded)	18.50%	34.50%

Chapter V – Conclusions

In this chapter, the research questions proposed in chapter I are answered by a short conclusion of the work presented on the appended papers.

Q1: To what extent can graphene maintain its structural and functional integrity after wear testing to function as a solid lubricant in wear resistant thermal spray coatings?

- The incorporation of graphene nanoplatelets into alumina thermal spray coatings successfully enhanced wear resistance, as evidenced by reduced CoF and specific wear rates. A degradation of the properties was seen with time during ball-on-disk testing.
- STXM and XANES analysis performed in synchrotron beamlines confirmed the retention of the GNP in the post wear sample. Ball-on disk wear testing affected the graphene-containing alumina coating. Below the wear track the material became amorphous and the GNPs were partly destroyed, seen with the high carbon content in the amorphous phase.
- GNPs were still found at the surface of the sample and were oriented parallel to the sliding direction. This confirms the ability of GNPs to act as a solid lubricant in wear resistant conditions.

Q2: How effective is a molecular-level mixing process in achieving controllable graphene coatings on metal powder composites?

- A molecular-level mixing process was successfully developed to coat graphene oxide onto pure copper powders, using APTES as a coupling agent.
- Two different parameters were varied to identify the ability of the process to tailor the characteristics of the GO coating. The APTES concentration during the surface functionalization step, and the GO solution concentration during the incorporation phase.
- The APTES concentration has been found to be a crucial factor in determining the coverage of the coating. At lower concentrations, partial coverage of the coating is produced, leaving part of the powder surface exposed. Between 0.2 and 0.8 vol% a thin and fully coated powder is produced. At higher concentrations, graphene accumulation begins to occur.

- GO solution concentration also played a role in both coverage and thickness of the coating. Lower concentrations lead to partial coverage, while higher concentrations achieve saturation. The controllability of the coating thickness were found in GO solution concentrations from 0.04 wt% to 0.167 wt%

Q3: Can the GO coated powder synthesized by the molecular-level mixing process be used to produce graphene containing wear resistance coatings via thermal spraying?

- The GO-coated WC-Co-Cr powder synthesized through the molecular-level mixing process was successfully processed into coatings via thermal spraying.
- The process demonstrated versatility by effectively coating porous powders, with GO detected on both external and internal surfaces of the pores.
- Wear testing using a ball-on-disc tribometer showed improved performance for the GO-coated coatings, with consistently reduced CoF throughout the test duration.
- XPS analysis confirmed the presence of GO in wear tracks across various conditions, including as-sprayed and ground samples, confirming the reliability of the developed process on GO retention under drastic wear conditions.

Chapter VI – Future work

This thesis presented a comprehensive investigation of graphene-based materials incorporated into thermal spray coatings. Besides the progress made, some knowledge gaps were identified, offering opportunities for future research. These gaps are outlined below to encourage further advancements in the field.

- The orientation of GNPs after the wear testing would be of interest to better understand the lubrication mechanisms.
- To enhance the friction-reducing capabilities of GO-containing WC-Co-Cr thermal spraying coatings, the GO content in the pores needs to be increased.
- To gain a deeper understanding of the mechanisms responsible for the change in GO's behavior in long-duration ball-on-disk experiments, further investigations are required.

References

[1] L. Zhang, Q. Ye, X. Zeng, S. Liu, H. Chen, Y. Tao, X. Yu, X. Wang, Preparation and Properties of Graphene Reinforced Copper Electrical Contact Materials for High-Voltage Direct Current Electrical Contacts, Electronics (Switzerland) 13 (2024). https://doi.org/10.3390/electronics13010053.

[2] D.K. Das, P.K. Swain, S. Sahoo, Graphene in turbine blades, Modern Physics Letters B 30 (2016). https://doi.org/10.1142/S0217984916502626.

[3] V.B. Mbayachi, E. Ndayiragije, T. Sammani, S. Taj, E.R. Mbuta, A. ullah khan, Graphene synthesis, characterization and its applications: A review, Results Chem 3 (2021). https://doi.org/10.1016/j.rechem.2021.100163.

[4] O. Guler, N. Bagci, A short review on mechanical properties of graphene reinforced metal matrix composites, Journal of Materials Research and Technology 9 (2020) 6808–6833. https://doi.org/10.1016/j.jmrt.2020.01.077.

[5] M. Kukielski, W. Bulejak, P. Wiecinska, L. Stobinski, W. Slubowska, M. Szafran, Graphene-reinforced ceramics obtained by slip casting and pressureless sintering: Interactions and stability of particles in aqueous environment, Open Ceramics 9 (2022). https://doi.org/10.1016/j.oceram.2022.100245.

[6] B. Sreenivasulu, R.B. R, M. Nagaral, ScienceDirect A Review on Graphene Reinforced Polymer Matrix Composites, 2017. www.sciencedirect.com.

[7] M. Cao, D.B. Xiong, Z. Tan, G. Ji, B. Amin-Ahmadi, Q. Guo, G. Fan, C. Guo, Z. Li, D. Zhang, Aligning graphene in bulk copper: Nacre-inspired nanolaminated architecture coupled with in-situ processing for enhanced mechanical properties and high electrical conductivity, Carbon N Y 117 (2017) 65–74. https://doi.org/10.1016/j.carbon.2017.02.089.

[8] H. Wang, H.M. Zhang, X.W. Cheng, S. Chang, X.N. Mu, Effect of ball milling time on microstructure and mechanical properties of graphene nanoplates and TiBw reinforced Ti–6Al–4V alloy composites, Materials Science and Engineering: A 861 (2022). https://doi.org/10.1016/j.msea.2022.144240.

[9] K. Derelizade, F. Venturi, R.G. Wellman, A. Kholobysov, T. Hussain, Wear performance of graphene nano platelets incorporated WC-Co coatings deposited by hybrid high velocity oxy fuel thermal spray, Wear 482–483 (2021). https://doi.org/10.1016/j.wear.2021.203974.

[10] S. Mahade, A. Mulone, S. Björklund, U. Klement, S. Joshi, Novel suspension route to incorporate graphene nano-platelets in HVAF-sprayed Cr3C2–NiCr coatings for superior wear performance, Journal of Materials Research and Technology 13 (2021) 498–512. https://doi.org/10.1016/j.jmrt.2021.04.096.

[11] K.S. Novoselov, A.K. Geim, S. V Morozov, D. Jiang, Y. Zhang, S. V Dubonos, I. V Grigorieva, A.A. Firsov, Electric Field Effect in Atomically Thin Carbon Films, Kluwer, 2000. www.arXiv.org/quant-ph/.

[12] A.D. Pingale, S.U. Belgamwar, J.S. Rathore, The influence of graphene nanoplatelets (GNPs) addition on the microstructure and mechanical properties of Cu-GNPs composites fabricated by electro-co-deposition and powder metallurgy, in: Mater Today Proc, Elsevier Ltd, 2020: pp. 2062–2067. https://doi.org/10.1016/j.matpr.2020.02.728.

[13] A.K. Geim, K.S. Novoselov, The rise of graphene, n.d. www.nature.com/naturematerials.

[14] K. Chu, X. hu Wang, Y. biao Li, D. jian Huang, Z. rong Geng, X. long Zhao, H. Liu, H. Zhang, Thermal properties of graphene/metal composites with aligned graphene, Mater Des 140 (2018) 85–94. https://doi.org/10.1016/j.matdes.2017.11.048.

[15] A. Kausar, Graphene: Structure, properties, preparation, modification, and applications, in: Graphene to Polymer/Graphene Nanocomposites, Elsevier, 2022: pp. 1–24. https://doi.org/10.1016/b978-0-323-90937-2.00010-1.

[16] R.G. Zonov, K.G. Mikheev, A.A. Chulkina, I.A. Zlobin, G.M. Mikheev, Effect of laser power on the structure and specific surface area of laser-induced graphene, Diam Relat Mater 148 (2024). https://doi.org/10.1016/j.diamond.2024.111409.

[17] Z. Zhuang, Z. Liu, X. Chen, Q. Lin, B. Shen, S. Chen, Influence of defect degree on corrosion resistance of graphene coating on titanium alloy, Journal of Electroanalytical Chemistry 967 (2024). https://doi.org/10.1016/j.jelechem.2024.118460.

[18] M. Liu, K. Lin, M. Zhou, A. Wallwork, M.A. Bissett, R.J. Young, I.A. Kinloch, Mechanism of gas barrier improvement of graphene/polypropylene nanocomposites for new-generation light-weight hydrogen storage, Compos Sci Technol 249 (2024). https://doi.org/10.1016/j.compscitech.2024.110483.

[19] A. Mondal, A. Kumar Kundu, H. Shankar Biswas, P. Mandal, D.K. Maiti, S. Poddar, Optimizing dielectric and electrical properties of graphene oxide thin film with temperature tuning: Insights from impedance spectra analysis on insulator to semiconductor transition, Inorg Chem Commun (2024) 113016. https://doi.org/10.1016/j.inoche.2024.113016.

[20] R.G. Zonov, K.G. Mikheev, A.A. Chulkina, I.A. Zlobin, G.M. Mikheev, Effect of laser power on the structure and specific surface area of laser-induced graphene, Diam Relat Mater 148 (2024). https://doi.org/10.1016/j.diamond.2024.111409.

[21] M. Mazaheri, J. Payandehpeyman, M. Hedayatian, Agglomeration and interphase-influenced effective elastic properties of Metal/Graphene

nanocomposites: A developed mean-field model, Compos Struct 329 (2024). https://doi.org/10.1016/j.compstruct.2023.117762.

[22] Y. Hernandez, V. Nicolosi, M. Lotya, F.M. Blighe, Z. Sun, S. De, I.T. McGovern, B. Holland, M. Byrne, Y.K. Gun'ko, J.J. Boland, P. Niraj, G. Duesberg, S. Krishnamurthy, R. Goodhue, J. Hutchison, V. Scardaci, A.C. Ferrari, J.N. Coleman, High-yield production of graphene by liquid-phase exfoliation of graphite, Nat Nanotechnol 3 (2008) 563–568. https://doi.org/10.1038/nnano.2008.215.

[23] P. Sun, S. Kuga, M. Wu, Y. Huang, Exfoliation of graphite by dry ball milling with cellulose, Cellulose 21 (2014) 2469–2478. https://doi.org/10.1007/s10570-014-0264-9.

[24] X. Chen, J.F. Dobson, C.L. Raston, Vortex fluidic exfoliation of graphite and boron nitride, Chemical Communications 48 (2012) 3703–3705. https://doi.org/10.1039/c2cc17611d.

[25] T.N.J.I. Edison, R. Atchudan, N. Karthik, P. Chandrasekaran, S. Perumal, P. Arunachalam, P.B. Raja, M.G. Sethuraman, Y.R. Lee, Electrochemically exfoliated graphene sheets as electrode material for aqueous symmetric supercapacitors, Surf Coat Technol 416 (2021). https://doi.org/10.1016/j.surfcoat.2021.127150.

[26] W.S. Hummers, R.E. Offeman, Preparation of Graphitic Oxide, 1958. https://pubs.acs.org/sharingguidelines.

[27] M. Bahiraei, S. Heshmatian, Graphene family nanofluids: A critical review and future research directions, Energy Convers Manag 196 (2019) 1222–1256. https://doi.org/10.1016/j.enconman.2019.06.076.

[28] A. Sandin, J.E. Rowe, D.B. Dougherty, Improved graphene growth in UHV: Pit-free surfaces by selective Si etching of SiC(0001)-Si with atomic hydrogen, Surf Sci 611 (2013) 25–31. https://doi.org/10.1016/j.susc.2013.01.010.

[29] M.Y. Lin, W.C. Guo, M.H. Wu, P.Y. Wang, S.C. Lee, S.Y. Lin, Graphene films grown at low substrate temperature and the growth model by using MBE technique, J Cryst Growth 378 (2013) 333–336. https://doi.org/10.1016/j.jcrysgro.2012.12.068.

[30] M.R. Anisur, R.K.S. Raman, P.C. Banerjee, S. Al-Saadi, A.K. Arya, Review of the role of CVD growth parameters on graphene coating characteristics and the resulting corrosion resistance, Surf Coat Technol 487 (2024). https://doi.org/10.1016/j.surfcoat.2024.130934.

[31] S. Ou, C. Liu, R. Yang, W. Fan, Z. Xie, B. Li, T. Meng, C. Zou, D. Shu, Y. Tong, Supramolecular-driven construction of multilayered structure by modified hummers method for robust silicon anode, Energy Storage Mater 73 (2024). https://doi.org/10.1016/j.ensm.2024.103814.

[32] H. Korucu, Multi response optimization of synthesis of boron compounds by Dopting to graphene oxide in the Modified Hummers method, Materials

Science and Engineering: B 311 (2025). https://doi.org/10.1016/j.mseb.2024.117839.

[33] A.U. Anuar, N.N. Bonnia, N.M. Jamil, N.D.N. Affandi, Graphene oxide based regenerated carbon waste tyre (rCB): Synthesis by modified Hummers method and characterization, Mater Today Proc (2023). https://doi.org/10.1016/j.matpr.2023.02.280.

[34] A.M. Dimiev, J.M. Tour, Mechanism of graphene oxide formation, ACS Nano 8 (2014) 3060–3068. https://doi.org/10.1021/nn500606a.

[35] S. Pan, I.A. Aksay, Factors controlling the size of graphene oxide sheets produced via the graphite oxide route, ACS Nano 5 (2011) 4073–4083. https://doi.org/10.1021/nn200666r.

[36] O.C. Compton, S.T. Nguyen, Graphene oxide, highly reduced graphene oxide, and graphene: Versatile building blocks for carbon-based materials, Small 6 (2010) 711–723. https://doi.org/10.1002/smll.200901934.

[37] U. Hofmann, R. Holst, Über die Säurenatur und die Methylierung von Graphitoxyd, Eur J Inorg Chem 72 (1939) 754–771. https://doi.org/10.1002/cber.19390720417.

[38] G. Ruess, Uber das Graphitoxyhydroxyd (Graphitoxyd), n.d.

[39] W. Scholz, H.P. Boehm, Untersuchungen am Graphitoxid. VI. Betrachtungen zur Struktur des Graphitoxids, ZAAC - Journal of Inorganic and General Chemistry 369 (1969) 327–340. https://doi.org/10.1002/zaac.19693690322.

[40] T. Nakajima, Y. Matsuo, FORMATION PROCESS AND STRUCTURE OF GRAPHITE OXIDE, 1994.

[41] H. He, T. Riedl, A. Lerf, J. Klinowski, Solid-State NMR Studies of the Structure of Graphite Oxide, 1996. https://pubs.acs.org/sharingguidelines.

[42] D.R. Dreyer, S. Park, C.W. Bielawski, R.S. Ruoff, The chemistry of graphene oxide, Chem Soc Rev 39 (2010) 228–240. https://doi.org/10.1039/b917103g.

[43] A. Lerf, H. He, M. Forster, J. Klinowski, Structure of Graphite Oxide Revisited |, 1998. https://pubs.acs.org/sharingguidelines.

[44] S. Guo, S. Garaj, A. Bianco, C. Ménard-Moyon, Controlling covalent chemistry on graphene oxide, Nature Reviews Physics 4 (2022) 247–262. https://doi.org/10.1038/s42254-022-00422-w.

[45] A. Jiříčková, O. Jankovský, Z. Sofer, D. Sedmidubský, Synthesis and Applications of Graphene Oxide, Materials 15 (2022). https://doi.org/10.3390/ma15030920.

[46] A.N. Ghulam, O.A.L. Dos Santos, L. Hazeem, B.P. Backx, M. Bououdina, S. Bellucci, Graphene Oxide (GO) Materials—Applications and Toxicity on Living Organisms and Environment, J Funct Biomater 13 (2022). https://doi.org/10.3390/jfb13020077.

[47] M. Kalbacova, A. Broz, J. Kong, M. Kalbac, Graphene substrates promote adherence of human osteoblasts and mesenchymal stromal cells, Carbon N Y 48 (2010) 4323–4329. https://doi.org/10.1016/j.carbon.2010.07.045.

[48] M. Lundie, Ž. Šljivančanin, S. Tomić, Electronic and optical properties of reduced graphene oxide, J Mater Chem C Mater 3 (2015) 7632–7641. https://doi.org/10.1039/c5tc00437c.

[49] I.A. Vacchi, C. Spinato, J. Raya, A. Bianco, C. Ménard-Moyon, Chemical reactivity of graphene oxide towards amines elucidated by solid-state NMR, Nanoscale 8 (2016) 13714–13721. https://doi.org/10.1039/c6nr03846h.

[50] Y. Liu, J. Wang, H. Zhang, C. Ma, J. Liu, S. Cao, X. Zhang, Enhancement of proton conductivity of chitosan membrane enabled by sulfonated graphene oxide under both hydrated and anhydrous conditions, J Power Sources 269 (2014) 898–911. https://doi.org/10.1016/j.jpowsour.2014.07.075.

[51] A.N. Ghulam, O.A.L. Dos Santos, L. Hazeem, B.P. Backx, M. Bououdina, S. Bellucci, Graphene Oxide (GO) Materials—Applications and Toxicity on Living Organisms and Environment, J Funct Biomater 13 (2022). https://doi.org/10.3390/jfb13020077.

[52] M. Mirzapour, P. Cousin, M. Robert, B. Benmokrane, Dispersion Characteristics, the Mechanical, Thermal Stability, and Durability Properties of Epoxy Nanocomposites Reinforced with Carbon Nanotubes, Graphene, or Graphene Oxide, Polymers (Basel) 16 (2024). https://doi.org/10.3390/polym16131836.

[53] A. Liang, X. Jiang, X. Hong, Y. Jiang, Z. Shao, D. Zhu, Recent developments concerning the dispersion methods and mechanisms of graphene, Coatings 8 (2018). https://doi.org/10.3390/coatings8010033.

[54] W. Guo, G. Chen, Fabrication of graphene/epoxy resin composites with much enhanced thermal conductivity via ball milling technique, J Appl Polym Sci 131 (2014). https://doi.org/10.1002/app.40565.

[55] M. Tan, Y. Qin, J. Luo, Y. Wang, F. Zhang, X. Zhao, X. Lei, CuS loaded on reduced graphene oxide prepared by ball milling method as cathode material for high- power aqueous Cu-Al hybrid-ion batteries, Electrochim Acta 476 (2024). https://doi.org/10.1016/j.electacta.2023.143734.

[56] Y. Wang, X. Liu, Y. Chen, X. Cai, L. Zhou, High energy ball milling composite modification of Mg2Ni hydrogen storage alloy by graphene and MWCNTs, Int J Hydrogen Energy 50 (2024) 1562–1573. https://doi.org/10.1016/j.ijhydene.2023.10.125.

[57] J. Fu, C. Wei, W. Wang, J.L. Wei, J. Lv, Studies of structure and properties of graphene oxide prepared by ball milling, Materials Research Innovations 19 (2015) S1277–S1280. https://doi.org/10.1179/1432891715Z.0000000001486.

[58] M. Mahouri, V. Parvaneh, A. Dadrasi, G.S. Sabet, Optimization and Experimental Investigation of the Mechanical Properties of Copper/Graphene

Oxide/Epoxy Hybrid Nanocomposites, Mechanics of Composite Materials 60 (2024) 523–534. https://doi.org/10.1007/s11029-024-10207-0.

[59] R. Kant, K.K. Sharma, Hybrid material of α-Fe2O3 nanostructure with reduced graphene oxide: Enhanced dielectric and optical properties in relation to their composition and morphology, J Mol Struct 1282 (2023). https://doi.org/10.1016/j.molstruc.2023.135216.

[60] T. Guo, C. Bulin, Facile preparation of MgO/graphene oxide nanocomposite for efficient removal of aqueous Congo red: adsorption performance and interaction mechanism, Research on Chemical Intermediates 47 (2021) 945–971. https://doi.org/10.1007/s11164-020-04310-9.

[61] A. Liang, X. Jiang, X. Hong, Y. Jiang, Z. Shao, D. Zhu, Recent developments concerning the dispersion methods and mechanisms of graphene, Coatings 8 (2018). https://doi.org/10.3390/coatings8010033.

[62] L. Sánchez-López, B. Chico, I. Llorente, M.L. Escudero, R.M. Lozano, M.C. García-Alonso, Covalent immobilization of graphene oxide on biomedical grade CoCr alloy by an improved multilayer system assembly via Silane/GO bonding, Mater Chem Phys 287 (2022). https://doi.org/10.1016/j.matchemphys.2022.126296.

[63] Y. Chen, Y.W. Liu, Y. Xie, H.H. Zhang, X.Q. Du, Z. Zhang, Preparation of hydrophobic silane/graphene oxide composite coating implanted with benzotriazole to improve the anti-corrosion performance of copper, J Alloys Compd 893 (2022). https://doi.org/10.1016/j.jallcom.2021.162305.

[64] S. Seetharaman, J. Subramanian, R.A. Singh, W.L.E. Wong, M.L.S. Nai, M. Gupta, Mechanical Properties of Sustainable Metal Matrix Composites: A Review on the Role of Green Reinforcements and Processing Methods, Technologies (Basel) 10 (2022). https://doi.org/10.3390/technologies10010032.

[65] T. Xu, S. Zhou, S. Cui, N. Song, L. Shi, P. Ding, Three-dimensional carbon fiber-graphene network for improved thermal conductive properties of polyamide-imide composites, Compos B Eng 178 (2019). https://doi.org/10.1016/j.compositesb.2019.107495.

[66] S. Guo, X. Zhang, C. Shi, E. Liu, C. He, F. He, N. Zhao, In situ synthesis of high content graphene nanoplatelets reinforced Cu matrix composites with enhanced thermal conductivity and tensile strength, Powder Technol 362 (2020) 126–134. https://doi.org/10.1016/j.powtec.2019.11.121.

[67] A.M. Xavior, P.H. Kumar, Processing and Characterization Techniques of Graphene Reinforced Metal Matrix Composites (GRMMC); A Review, 2017. www.sciencedirect.comwww.materialstoday.com/proceedings2214-7853.

[68] T. Li, Y. Wang, M. Yang, H. Hou, S. Wu, High strength and conductivity copper/graphene composites prepared by severe plastic deformation of

graphene coated copper powder, Materials Science and Engineering: A 826 (2021). https://doi.org/10.1016/j.msea.2021.141983.

[69] K.A. Kowalsky, V.K. Champagne, M.F. Smith, Comparing cold spray with thermal spray coating technologies, in: Advances in Cold Spray: A Coating Deposition and Additive Manufacturing Process, Elsevier, 2023: pp. 43–63. https://doi.org/10.1016/B978-0-08-103015-8.00012-8.

[70] N. Espallargas, Introduction to thermal spray coatings, in: Future Development of Thermal Spray Coatings: Types, Designs, Manufacture and Applications, Elsevier Inc., 2015: pp. 1–13. https://doi.org/10.1016/B978-0-85709-769-9.00001-4.

[71] G.E. Kim, 3 Thermal Sprayed Nanostructured Coatings: Applications and Developments, 2007.

[72] R.K. Guduru, U. Dixit, A. Kumar, A critical review on thermal spray based manufacturing technologies, in: Mater Today Proc, Elsevier Ltd, 2022: pp. 7265–7269. https://doi.org/10.1016/j.matpr.2022.04.107.

[73] M. Daroonparvar, H.R. Bakhsheshi-Rad, A. Saberi, M. Razzaghi, A.K. Kasar, S. Ramakrishna, P.L. Menezes, M. Misra, A.F. Ismail, S. Sharif, F. Berto, Surface modification of magnesium alloys using thermal and solid-state cold spray processes: Challenges and latest progresses, Journal of Magnesium and Alloys 10 (2022) 2025–2061. https://doi.org/10.1016/j.jma.2022.07.012.

[74] W. Fan, Y. Bai, Review of suspension and solution precursor plasma sprayed thermal barrier coatings, Ceram Int 42 (2016) 14299–14312. https://doi.org/10.1016/j.ceramint.2016.06.063.

[75] JC. Tan, Hashmi M.S.J., HIGH VELOCITY OXYGEN FUEL (HVOF) THERMAL SPRAY: PROSPECT AND LIMITATION FOR ENGINEERING APPLICATION, in: Current Advances in Mechanical Design & Production, Sixth Cairo University International MDP Conference, Dublin, Ireland., 1996: pp. 2–4.

[76] W. Zhang, E.P.C. Lai, Chemical Functionalities of 3-aminopropyltriethoxy-silane for Surface Modification of Metal Oxide Nanoparticles, (n.d.). https://doi.org/10.1007/s12633-021-01477-7/Published.

[77] M. Sypabekova, A. Hagemann, D. Rho, S. Kim, Review: 3-Aminopropyltriethoxysilane (APTES) Deposition Methods on Oxide Surfaces in Solution and Vapor Phases for Biosensing Applications, Biosensors (Basel) 13 (2023). https://doi.org/10.3390/bios13010036.

[78] M. Sypabekova, A. Hagemann, D. Rho, S. Kim, Review: 3-Aminopropyltriethoxysilane (APTES) Deposition Methods on Oxide Surfaces in Solution and Vapor Phases for Biosensing Applications, Biosensors (Basel) 13 (2023). https://doi.org/10.3390/bios13010036.

[79] M.E. McGovern, K.M.R. Kallury, M. Thompson, Role of Solvent on the Silanization of Glass with Octadecyltrichlorosilane, Langmuir 10 (1994) 3607–3614. https://doi.org/10.1021/la00022a038.

[80] L. Marchetti, P. Mellin, C. Neil Hulme, Negative impact of humidity on the flowability of steel powders, Particulate Science and Technology 40 (2022) 722–736. https://doi.org/10.1080/02726351.2021.1995091.

[81] P. Mellin, T. Zavalis, L. Tingö, H. Brodin, J. Wendel, S. Berg, D. Riabov, A. Strondl, L. Nyborg, Moisture content analysis of metal powders using oven desorption followed by Karl Fischer titration, Metal Powder Report 75 (2020) 34–39. https://doi.org/10.1016/j.mprp.2019.04.002.

[82] A. Ganvir, S. Björklund, Y. Yao, S.V.S.S. Vadali, U. Klement, S. Joshi, A facile approach to deposit graphenaceous composite coatings by suspension plasma spraying, Coatings 9 (2019). https://doi.org/10.3390/coatings9030171.

[83] H. Pulikkalparambil, A. Babu, A. Thilak, N.P. Vighnesh, S. Mavinkere Rangappa, S. Siengchin, A review on sliding wear properties of sustainable biocomposites: Classifications, fabrication and discussions, Heliyon 9 (2023). https://doi.org/10.1016/j.heliyon.2023.e14381.

[84] H. Haider, D. Baykal, UHMWPE Biomaterials Handbook 30 Wear Assessment of UHMWPE with Pin-on-Disc Testing, 2016.

[85] K. Edalati, M. Ashida, Z. Horita, T. Matsui, H. Kato, Wear resistance and tribological features of pure aluminum and Al-Al2O3 composites consolidated by high-pressure torsion, Wear 310 (2014) 83–89. https://doi.org/10.1016/j.wear.2013.12.022.

[86] S. Mahade, A. Mulone, S. Björklund, U. Klement, S. Joshi, Incorporation of graphene nano platelets in suspension plasma sprayed alumina coatings for improved tribological properties, Appl Surf Sci 570 (2021). https://doi.org/10.1016/j.apsusc.2021.151227.

[87] X. Chen, X. Wang, D. Fang, A review on C1s XPS-spectra for some kinds of carbon materials, Fullerenes Nanotubes and Carbon Nanostructures (2020) 1048–1058. https://doi.org/10.1080/1536383X.2020.1794851.